Wireless Communications

Principles and Practice

2/e

T.S. Rapppaport

Chapter 6: Modulation Techniques for Mobile Radio

Analog and Digital Modulation, Line Coding, AM/FM/SSB

Digital Fundamentals: The Sampling Theorem, Nyquist Sampling

Key Digital Modulation Techniques: BPSK, OFDM, GMSK

Spread Spectrum: DS-SS, FH-SS, Coding Gain, Fading Margins

Amplitude Modulation

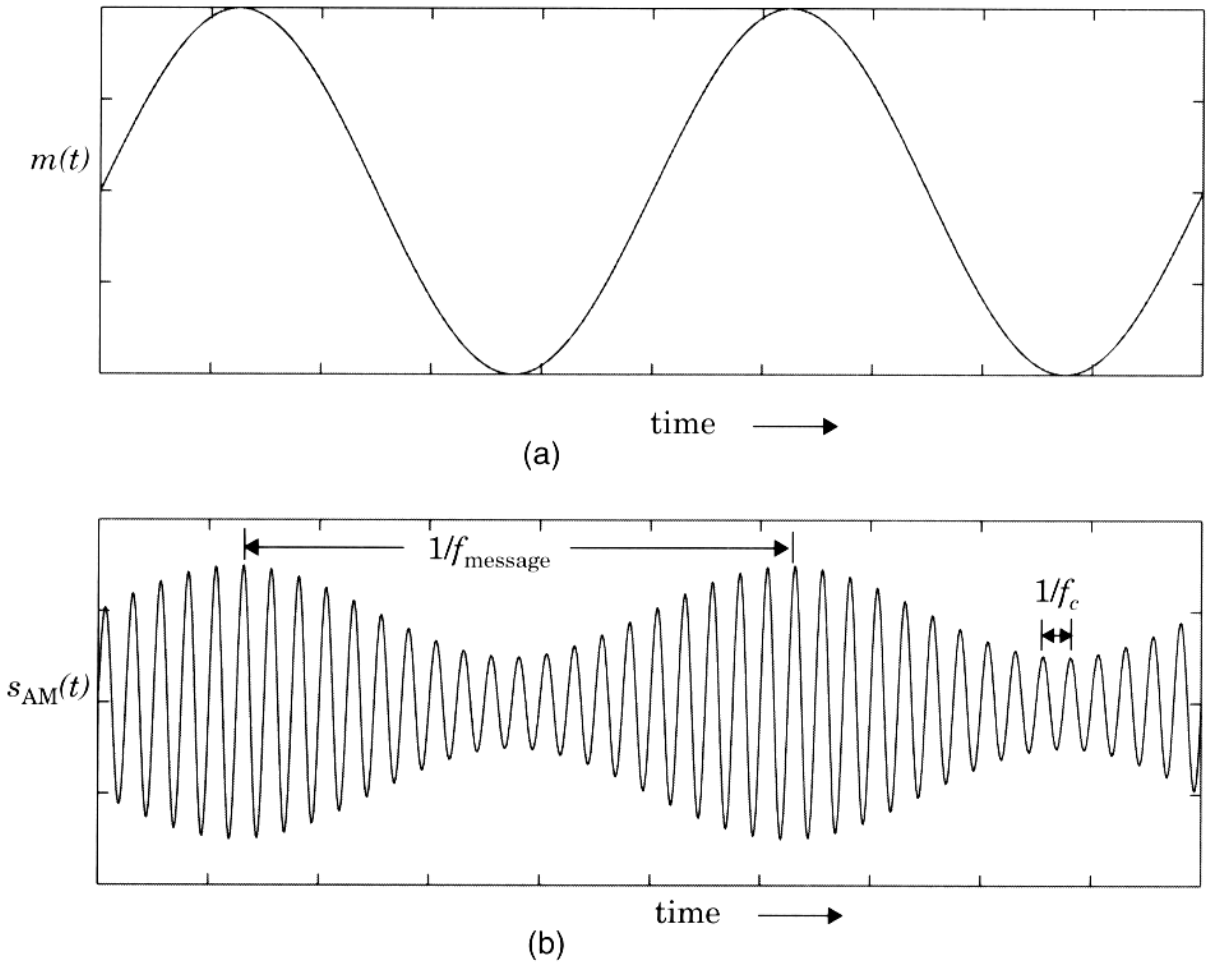

Figure 6.1 (a) A sinusoidal modulating signal and (b) the corresponding AM signal with modulation index 0.5.

Double Sideband Spectrum

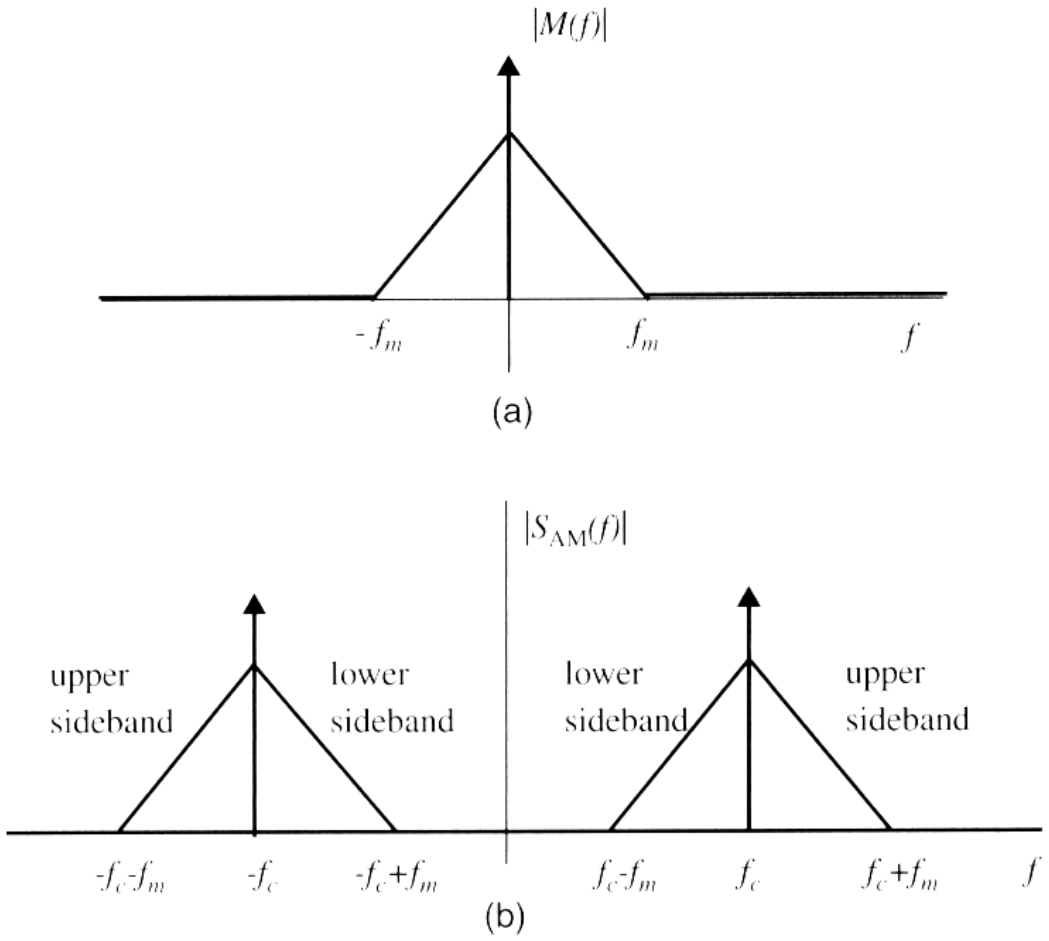

Figure 6.2 (a) Spectrum of a message signal; (b) spectrum of the corresponding AM signal.

SSB Modulators

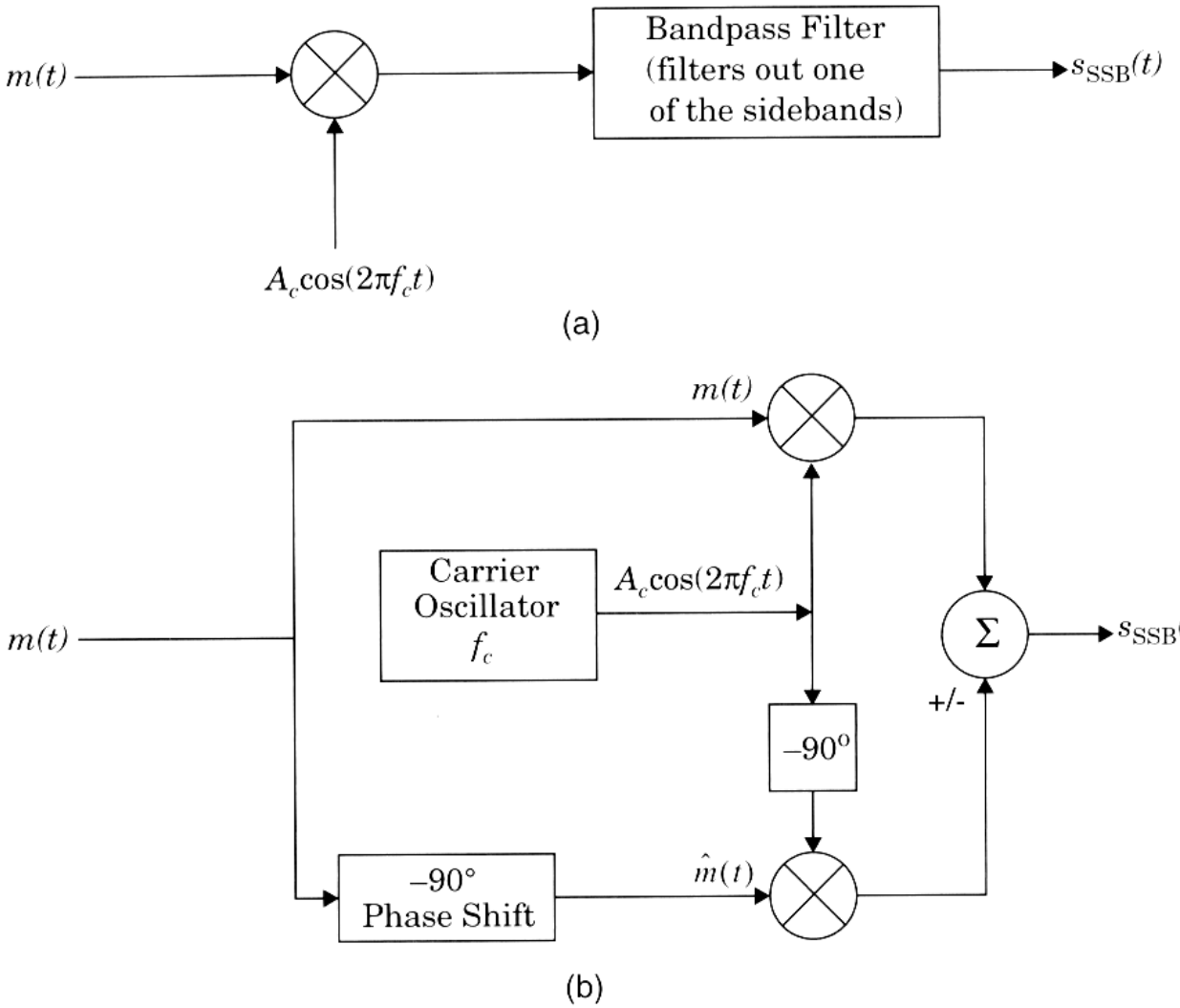

Figure 6.3 Generation of SSB using (a) a sideband filter and (b) a balanced modulator.

Tone-in Band SSB

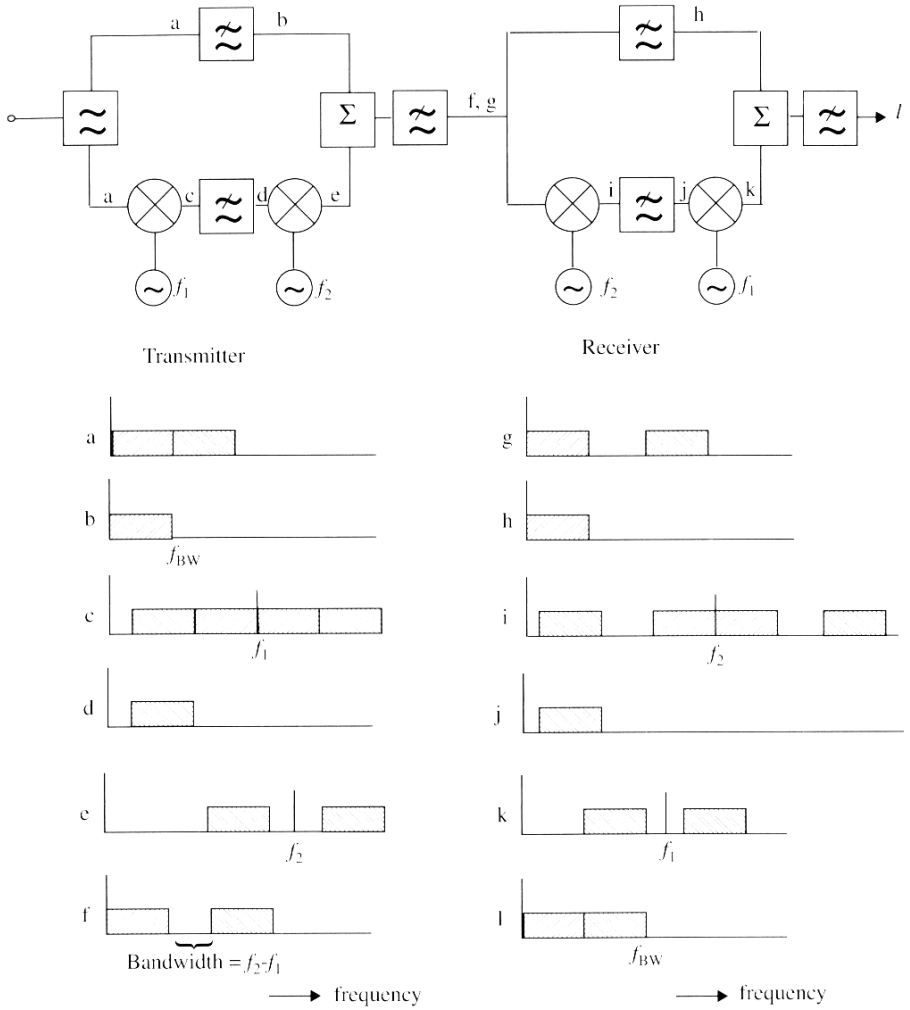

Figure 6.4 Illustration of transparent tone-in-band system [from [McG84] © IEEE]. Only positive frequencies are shown, and the two different cross-hatchings denote different spectral bands.

Product Detection

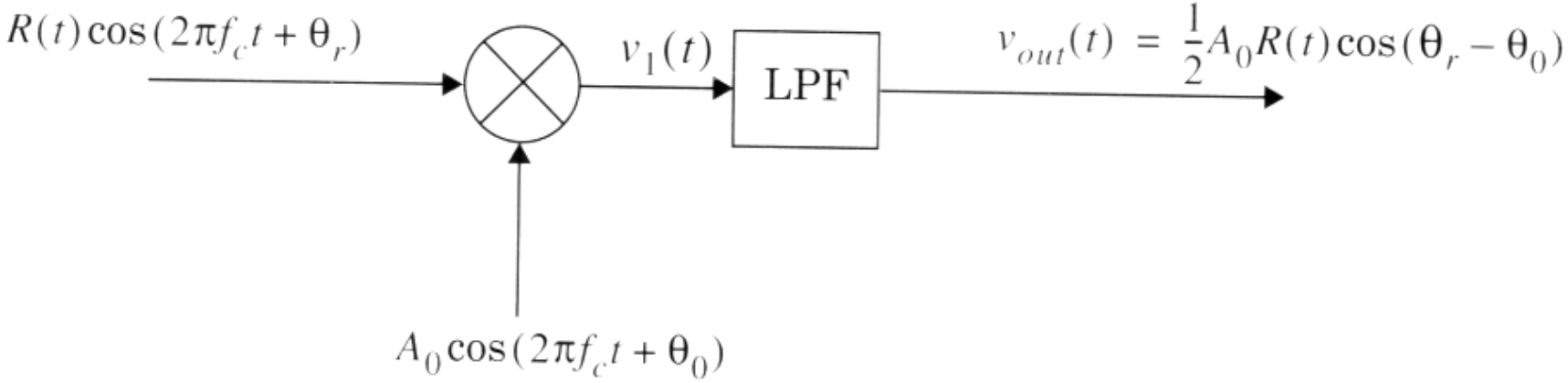

Figure 6.5 Block diagram of a product detector.

VCO circuit

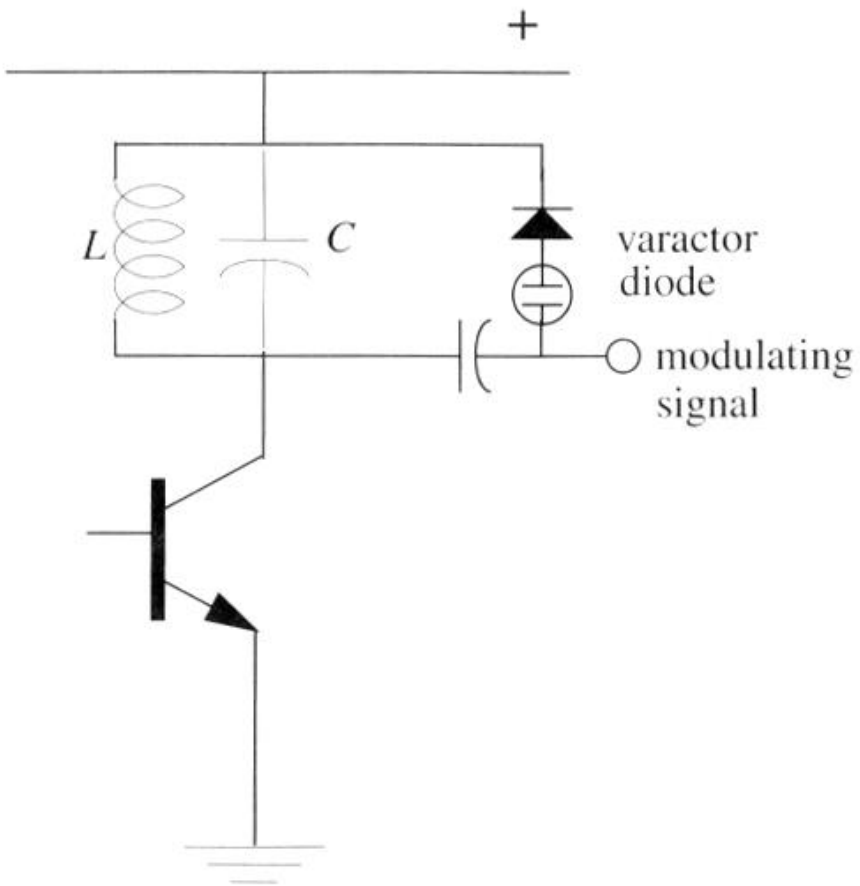

Figure 6.6 A simple reactance modulator in which the capacitance of a varactor diode is changed to vary the frequency of a simple oscillator. This circuit serves as a VCO.

Wideband FM generation

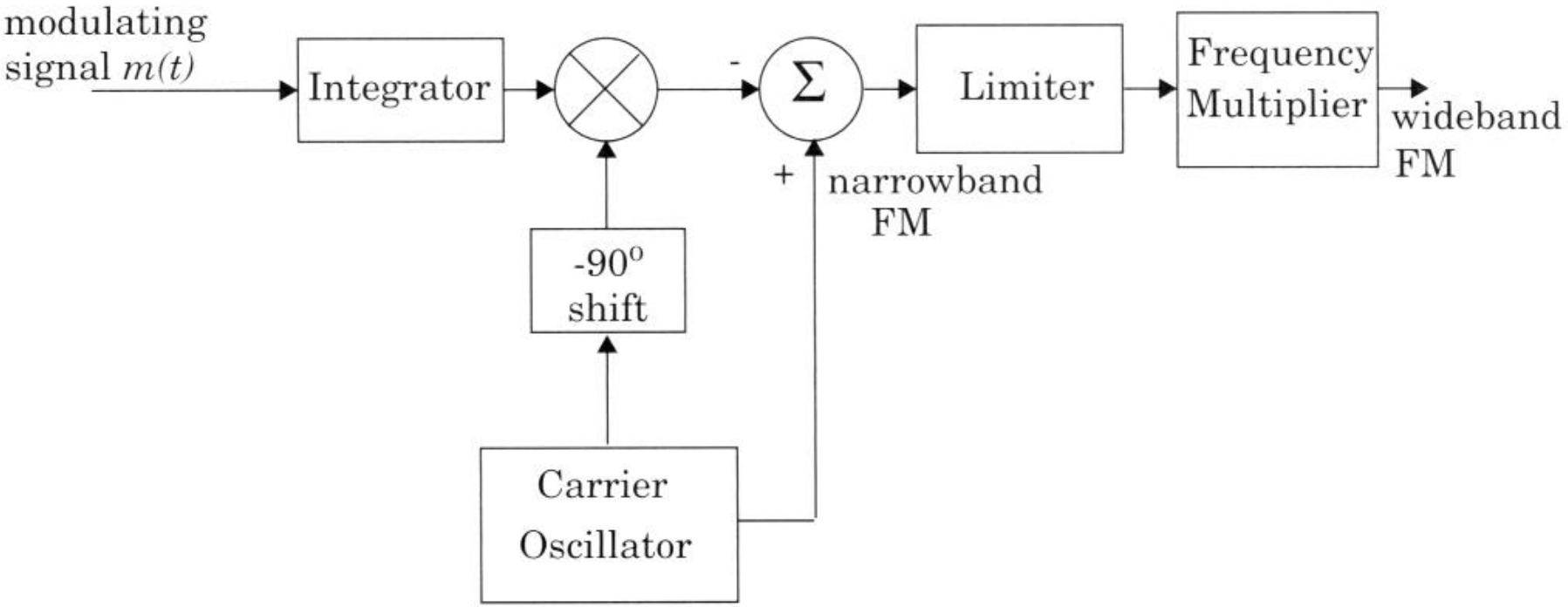

Figure 6.7 Indirect method for generating a wideband FM signal. A narrowband FM signal is generated using a balanced modulator and then frequency multiplied to generate a wideband FM signal.

Slope Detector for FM

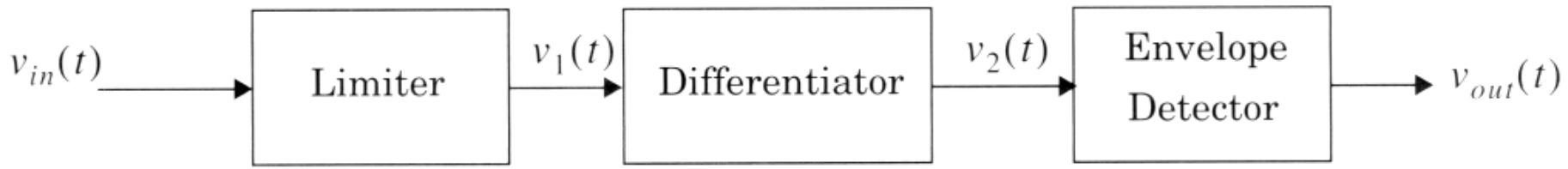

Figure 6.8 Block diagram of a slope detector type FM demodulator.

Digital Demod for FM

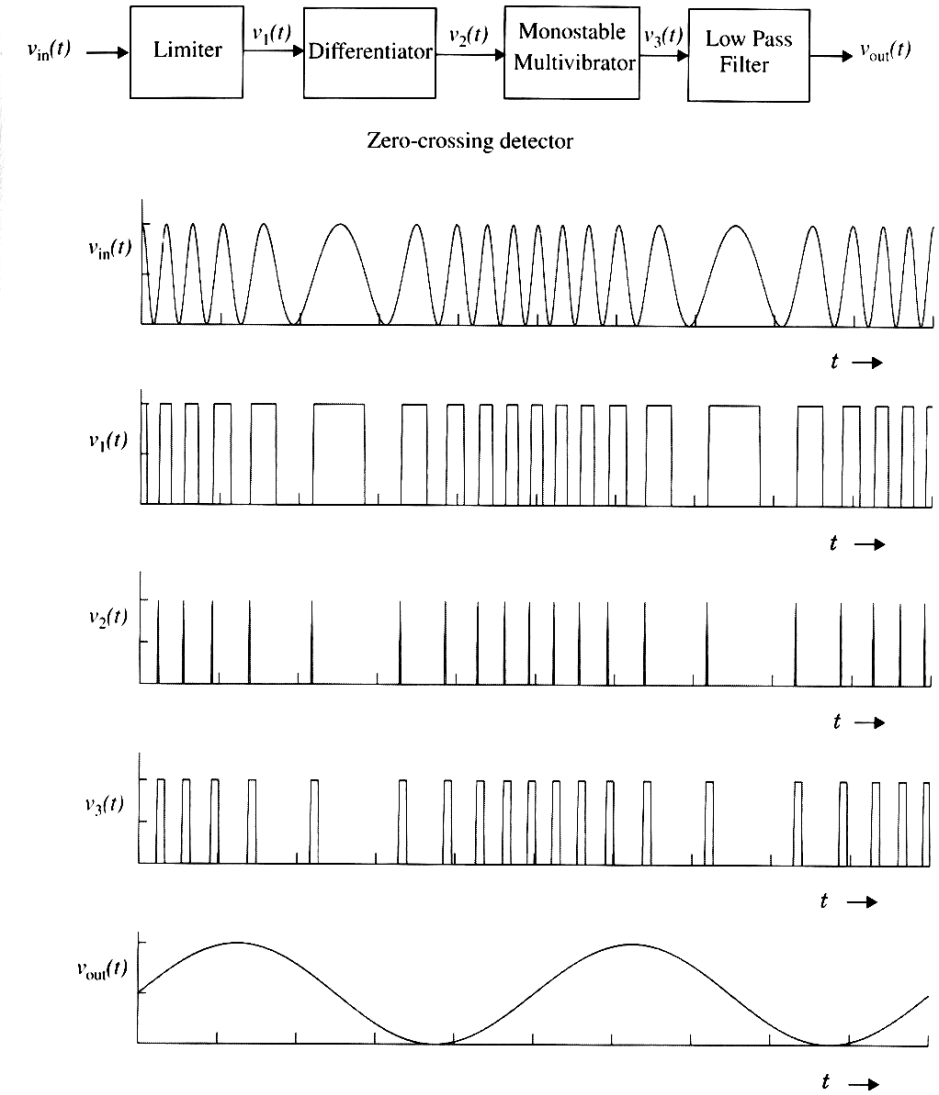

Figure 6.9 Block diagram of a zero-crossing detector and associated waveforms.

PLL Demod for FM

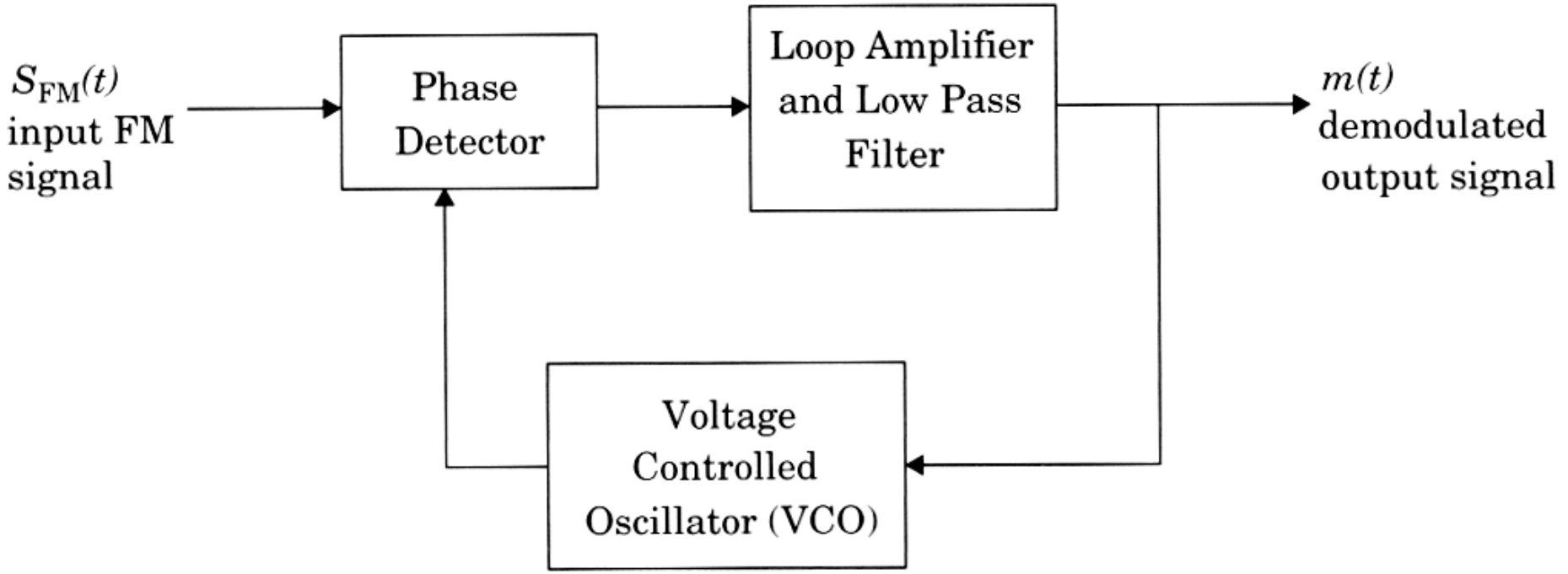

Figure 6.10 Block diagram of a PLL used as a frequency demodulator.

Phase-shift quadrature FM demod

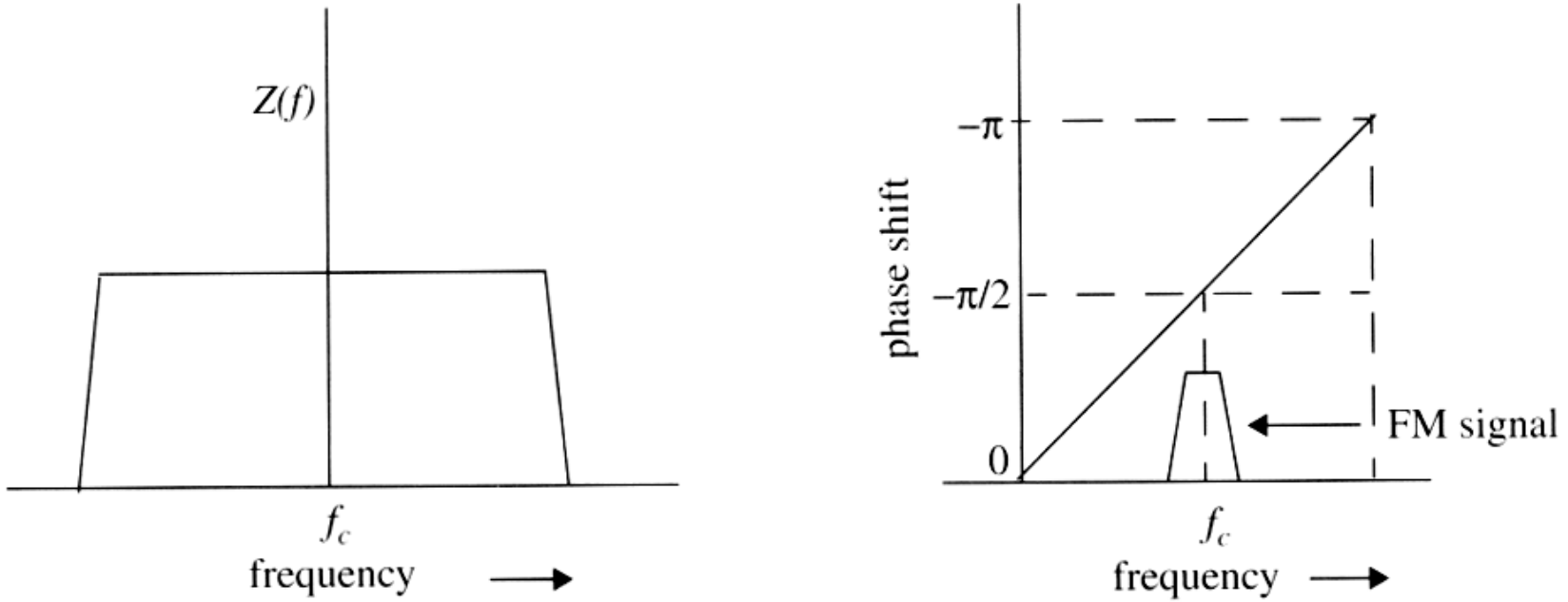

Figure 6.11 Characteristics of the phase-shift network with constant gain and linear phase.

FM Demod circuit

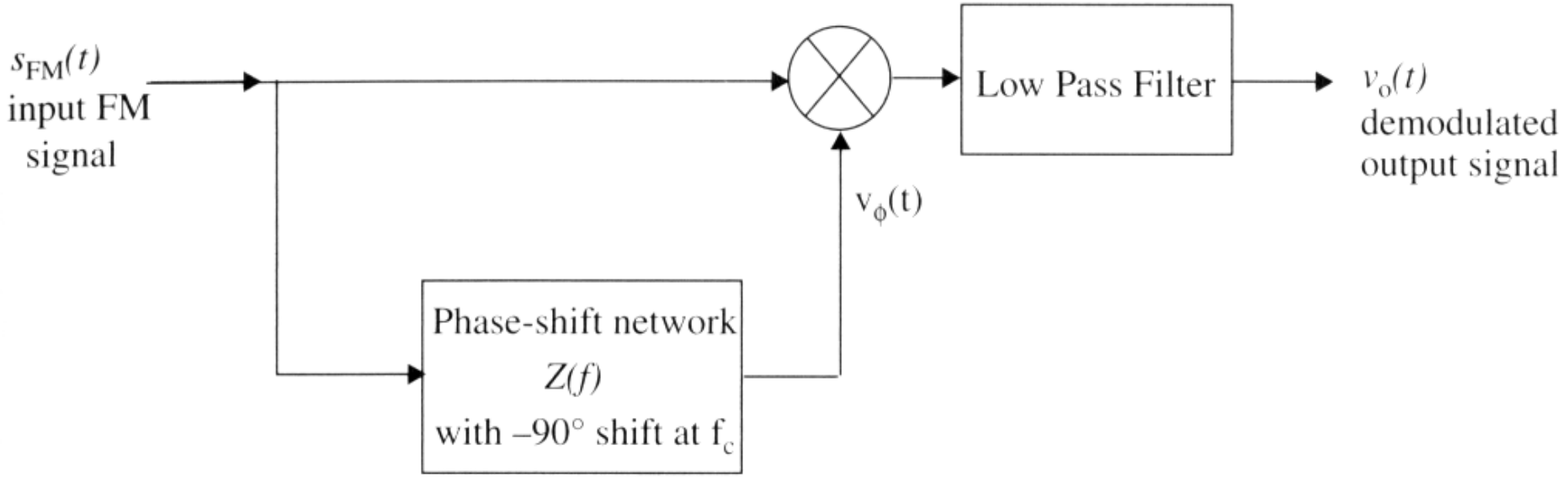

Figure 6.12 Block diagram of a quadrature detector.

Line Coding spectra

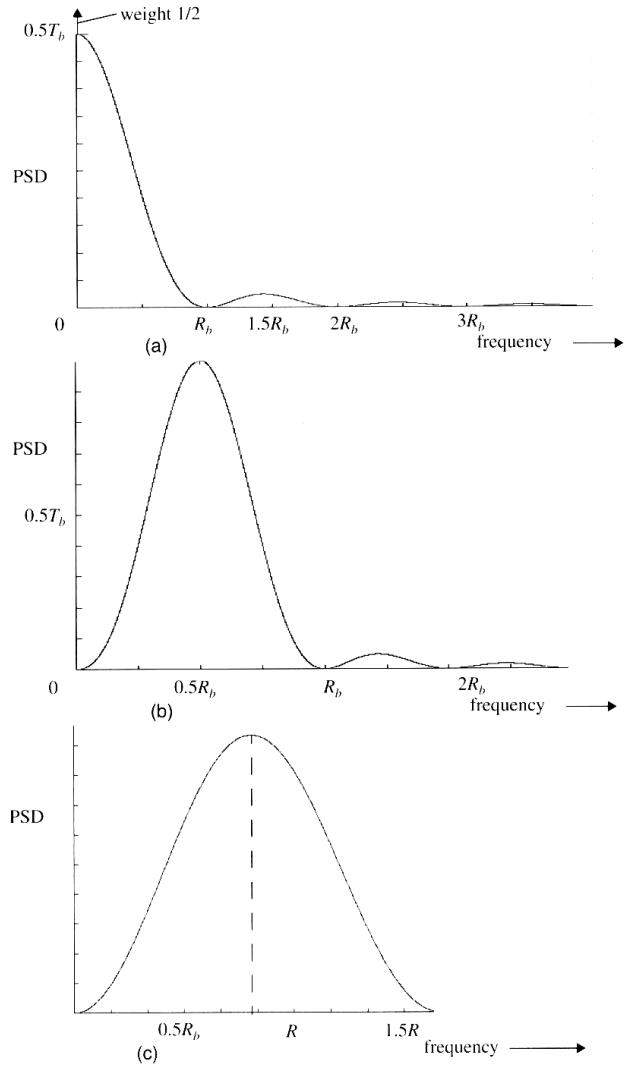

Figure 6.13 Power spectral density of (a) unipolar NRZ, (b) bipolar RZ, and (c) Manchester NRZ line codes.

RZ and NRZ Line Codes

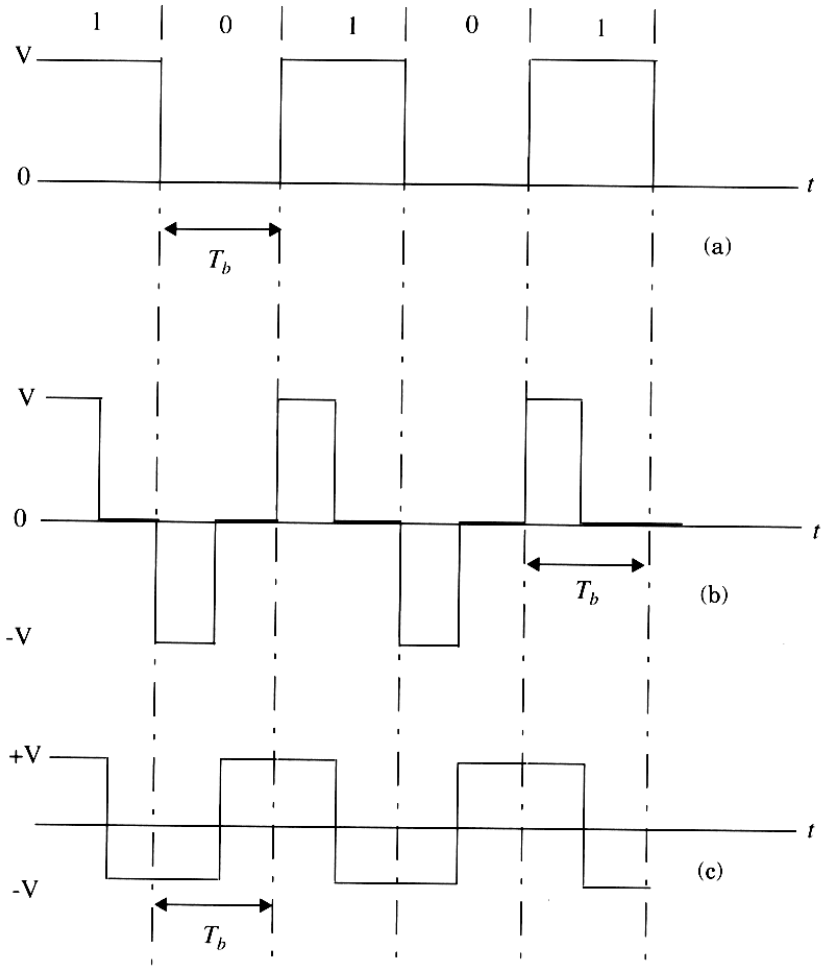

Figure 6.14 Time waveforms of binary line codes: (a) unipolar NRZ; (b) bipolar RZ; (c) Manchester NRZ.

Nyquist Pulses for zero-ISI

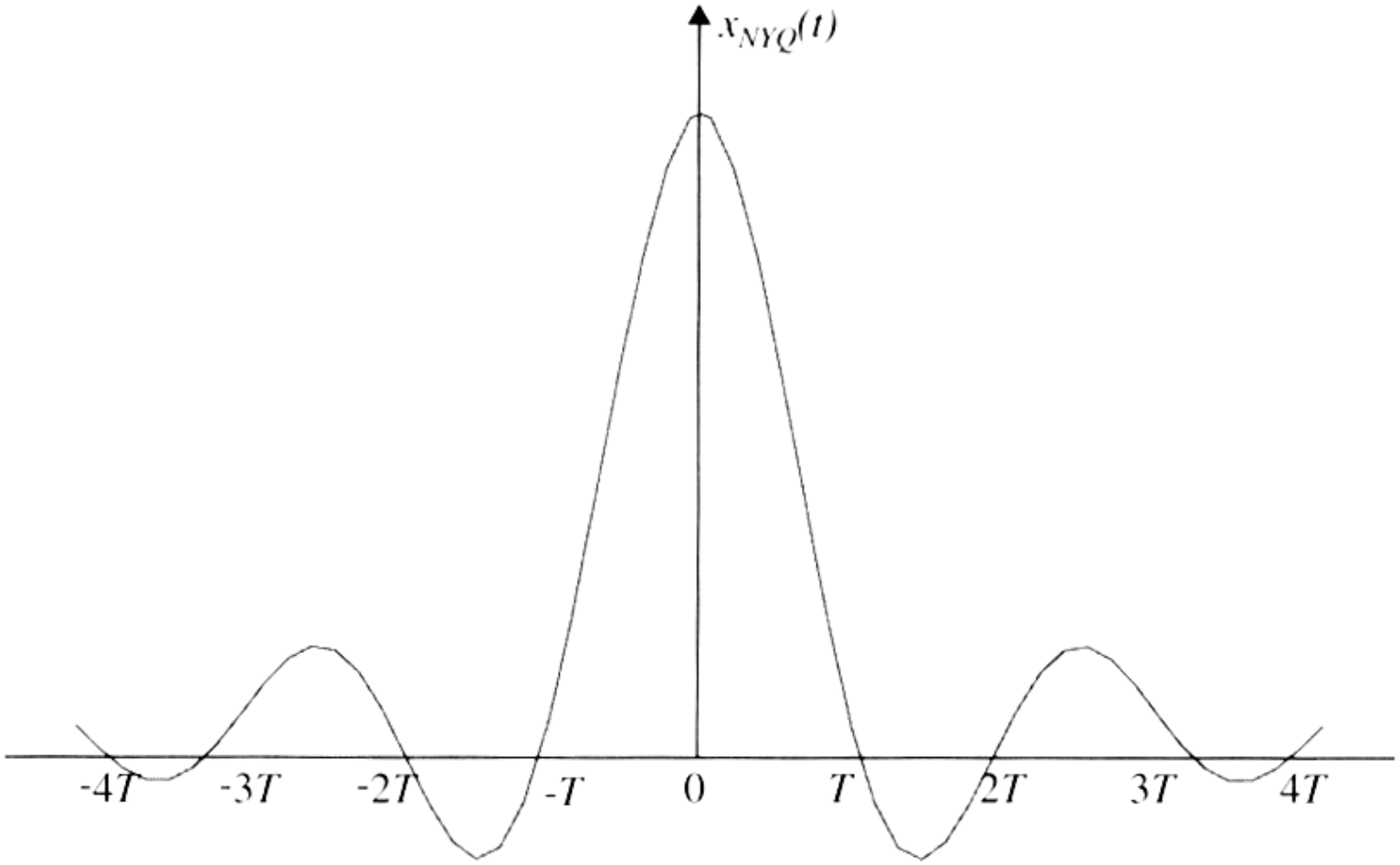

Figure 6.15 Nyquist ideal pulse shape for zero intersymbol interference.

Raised Cosine Spectrum

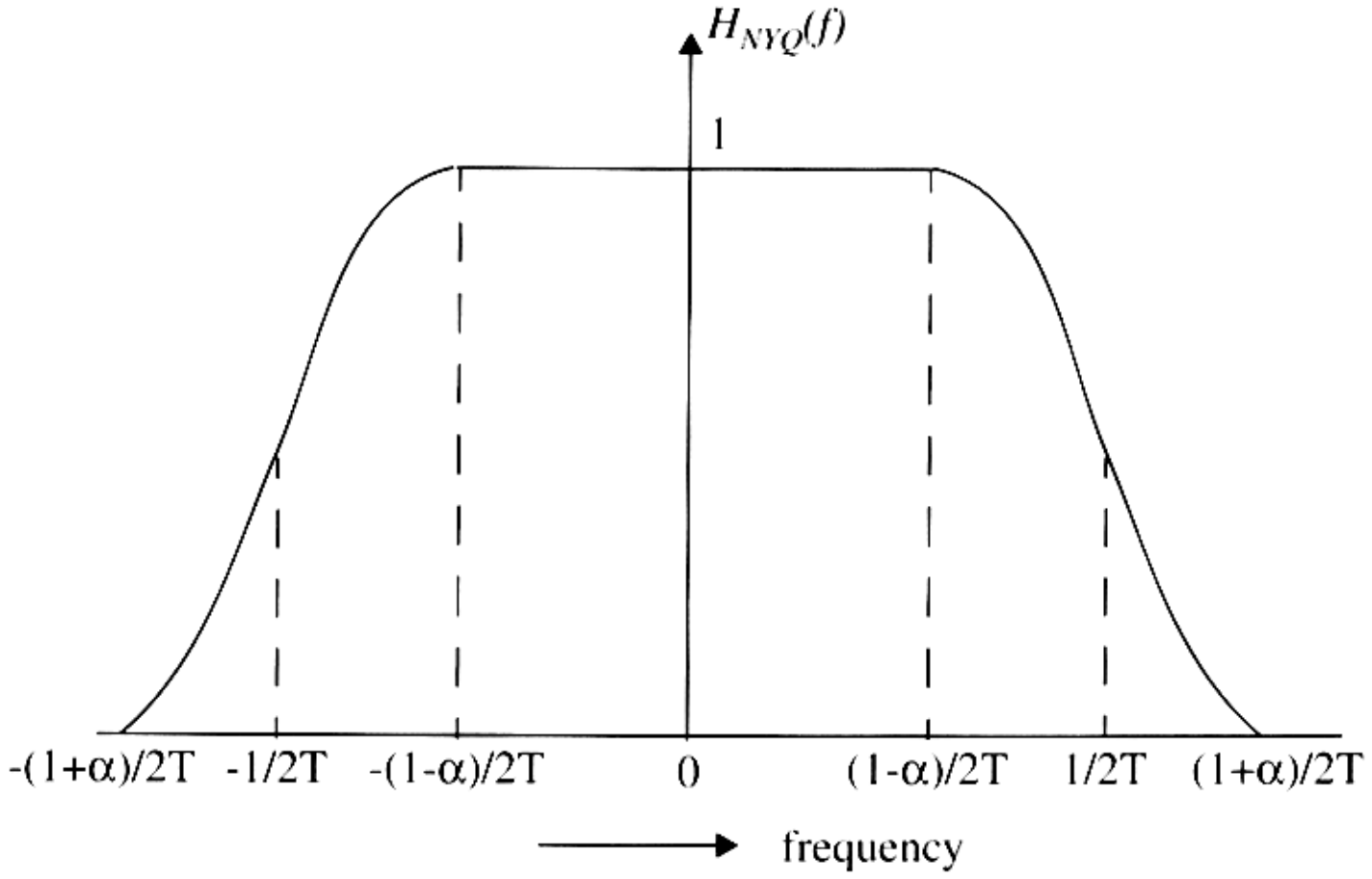

Figure 6.16 Transfer function of a Nyquist pulse-shaping filter at baseband.

Spectrum of Raised Cosine pulse

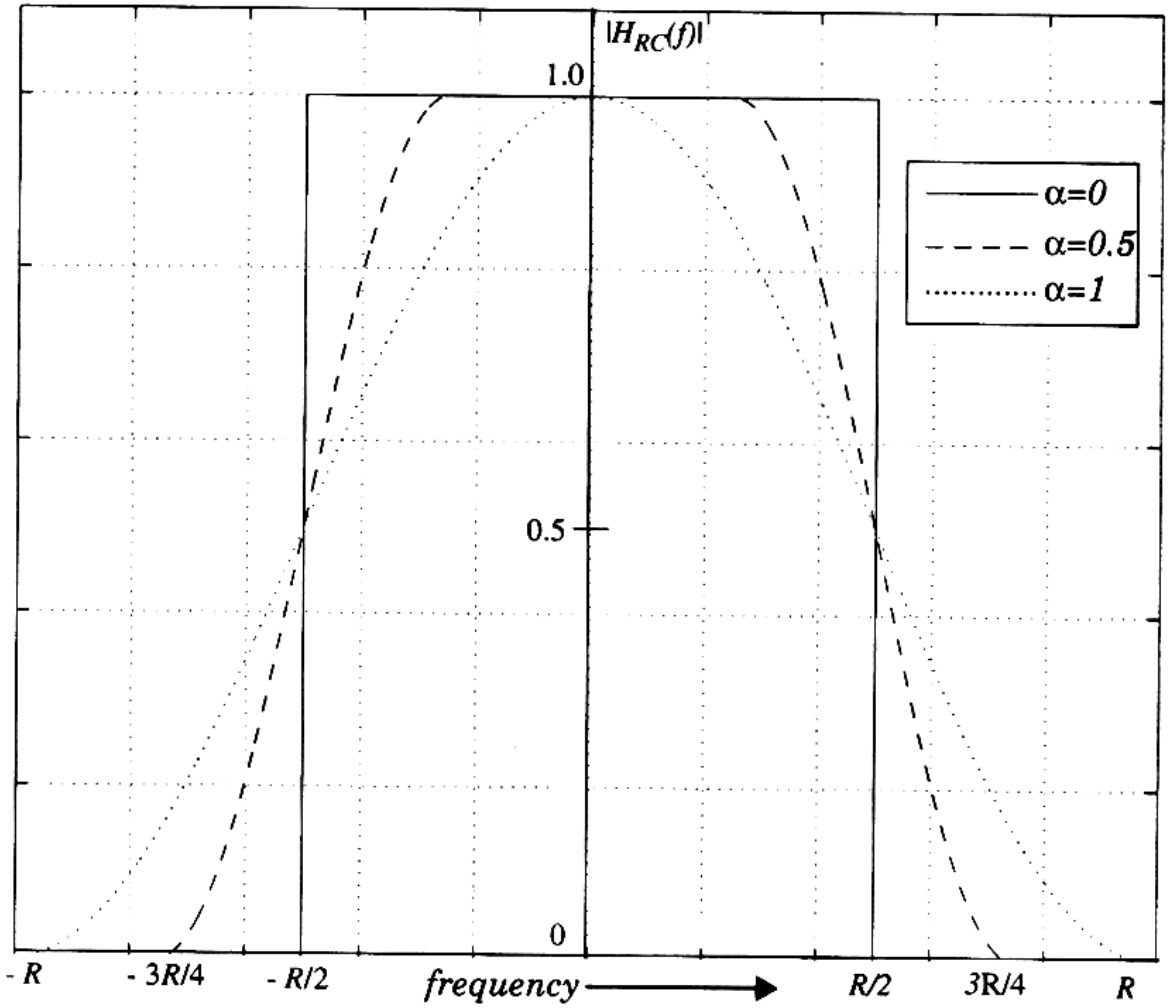

Figure 6.17 Magnitude transfer function of a raised cosine filter at baseband.

Raised Cosine pulses

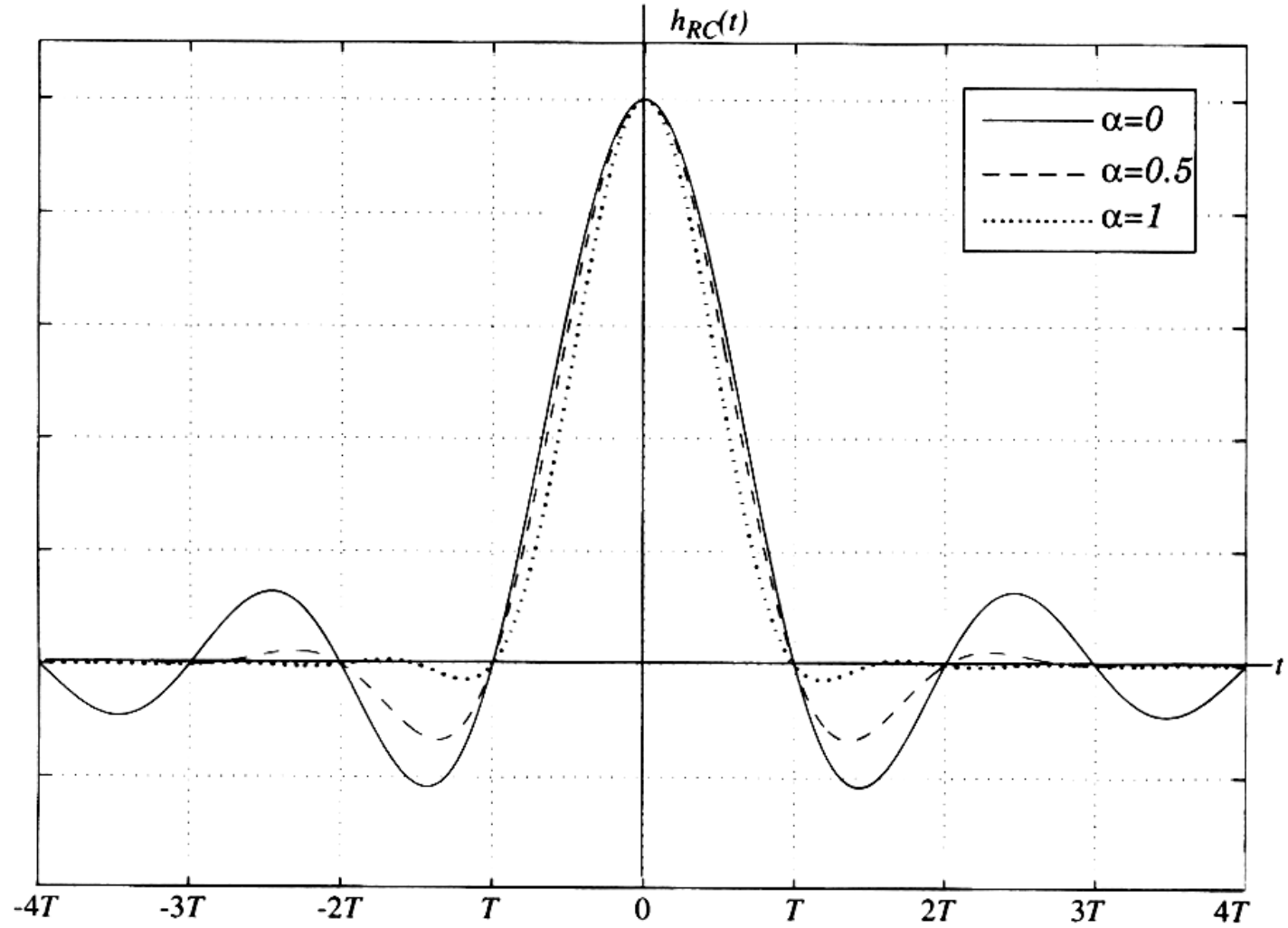

Figure 6.18 Impulse response of a raised cosine rolloff filter at baseband.

RF signal usig Raised Cosine

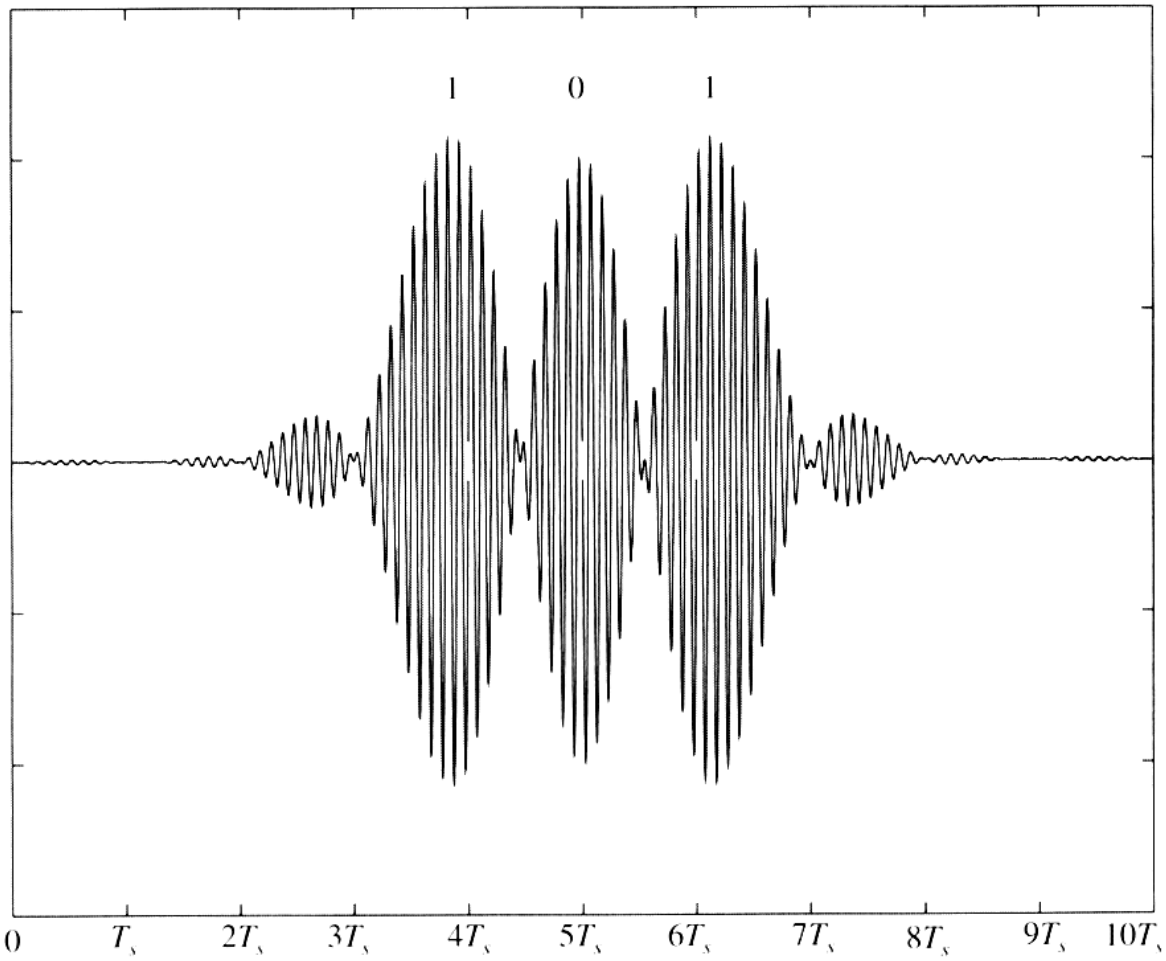

Figure 6.19 Raised cosine filtered ($\alpha = 0.5$) pulses corresponding to 1, 0, 1 data stream for a BPSK signal. Notice that the decision points (at $4T_s$, $5T_s$, $6T_s$) do not always correspond to the maximum values of the RF waveform.

Gaussian pulse-shapes

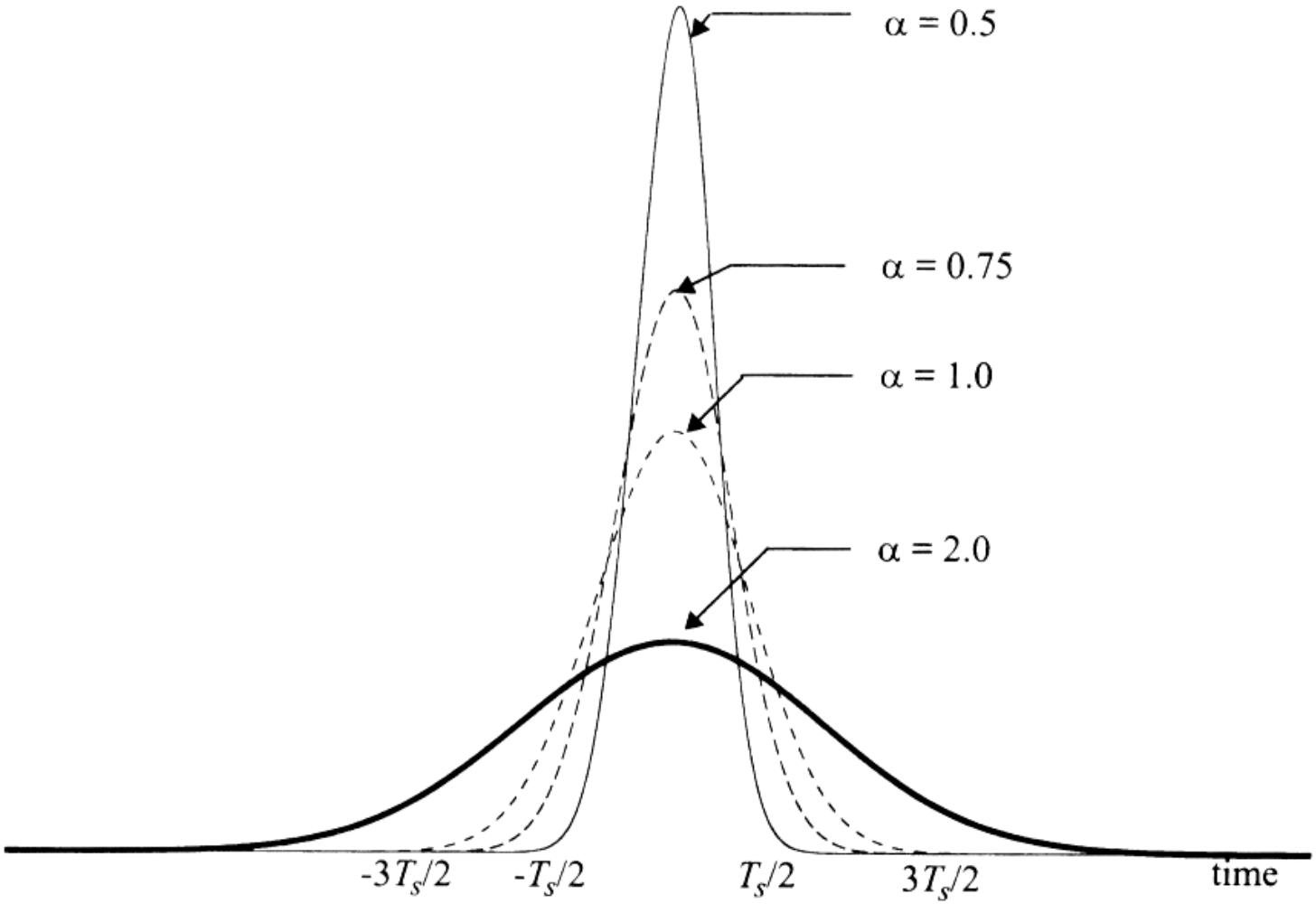

Figure 6.20 Impulse response of a Gaussian pulse-shaping filter.

BPSK constellation

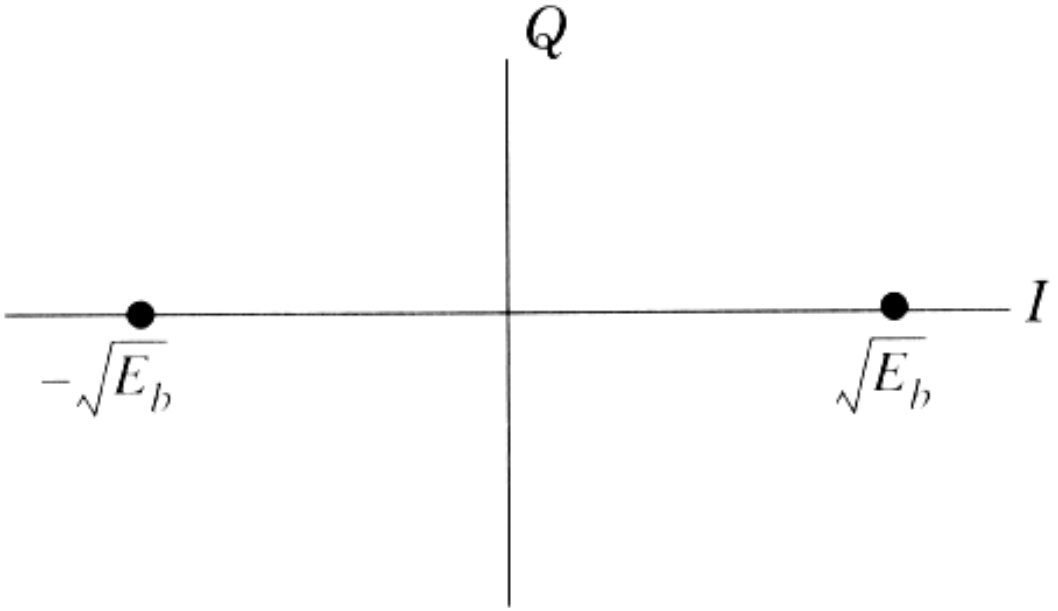

Figure 6.21 BPSK constellation diagram.

Virtue of pulse shaping

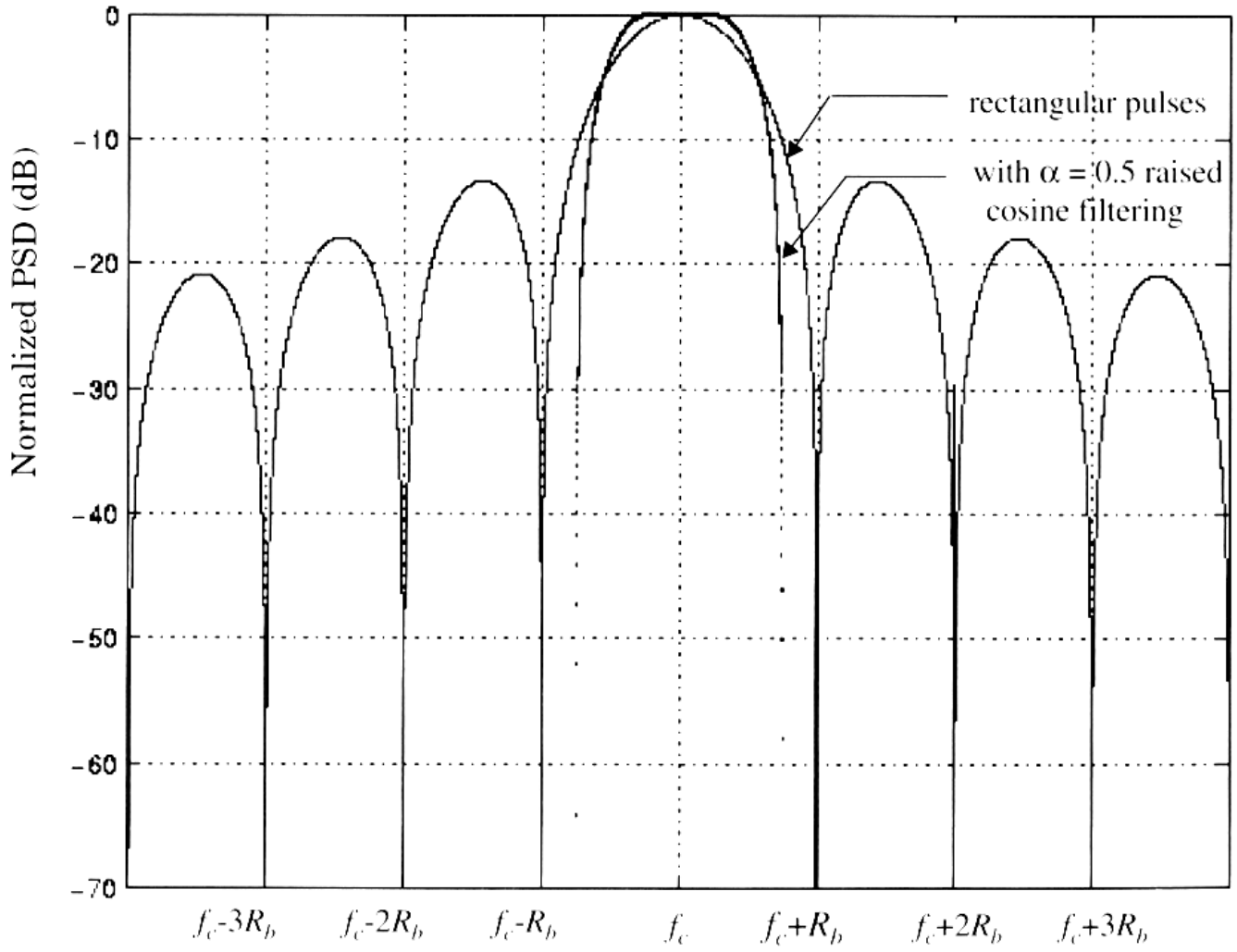

Figure 6.22 Power spectral density (PSD) of a BPSK signal.

BPSK Coherent demodulator

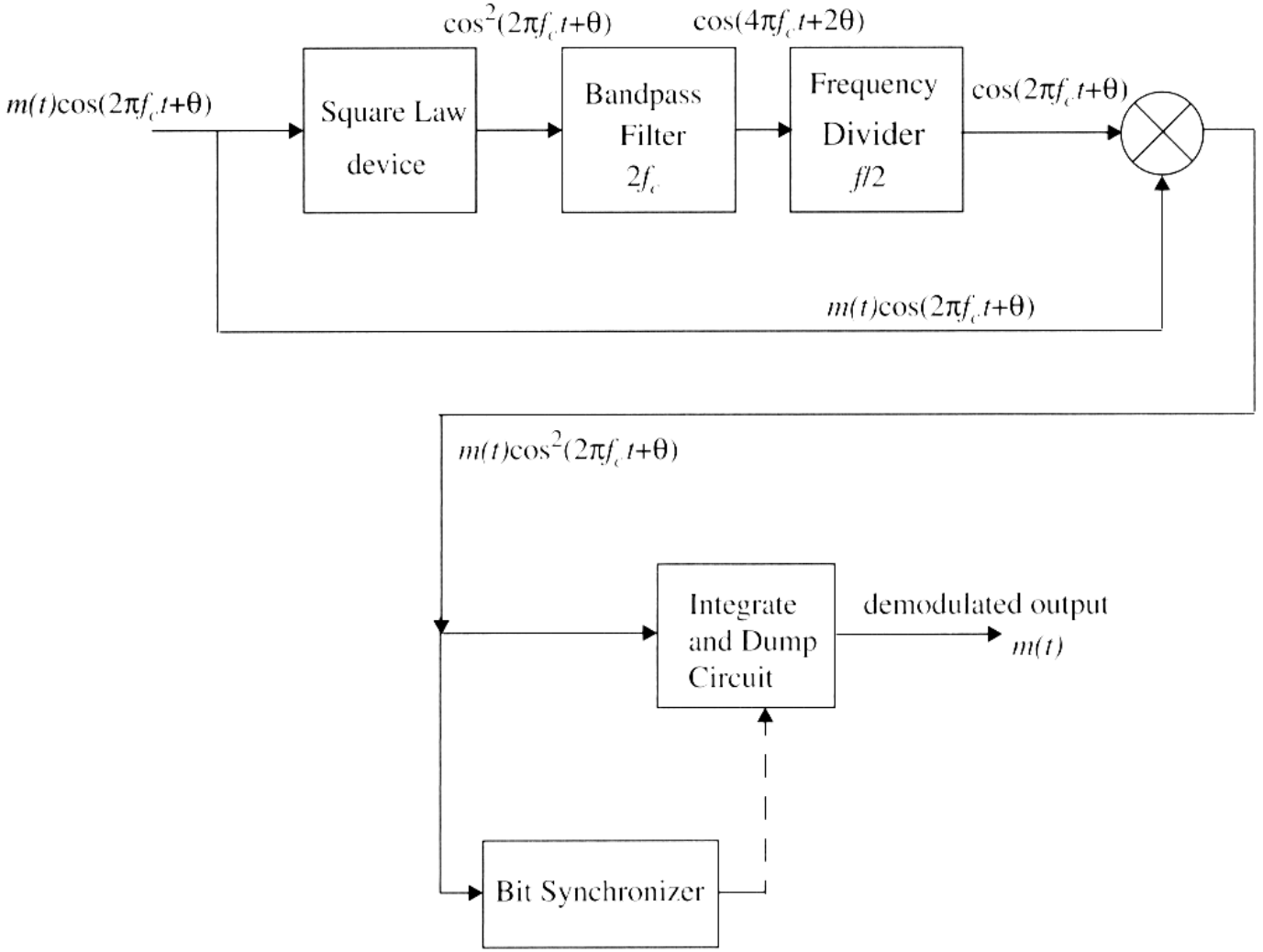

Figure 6.23 BPSK receiver with carrier recovery circuits.

Differential PSK encoding

Table 6.1 Illustration of the Differential Encoding Process

$\{m_k\}$		1	0	0	1	0	1	1	0
$\{d_{k-1}\}$		1	1	0	1	1	0	0	0
$\{d_k\}$	1	1	0	1	1	0	0	0	1

DPSK modulation

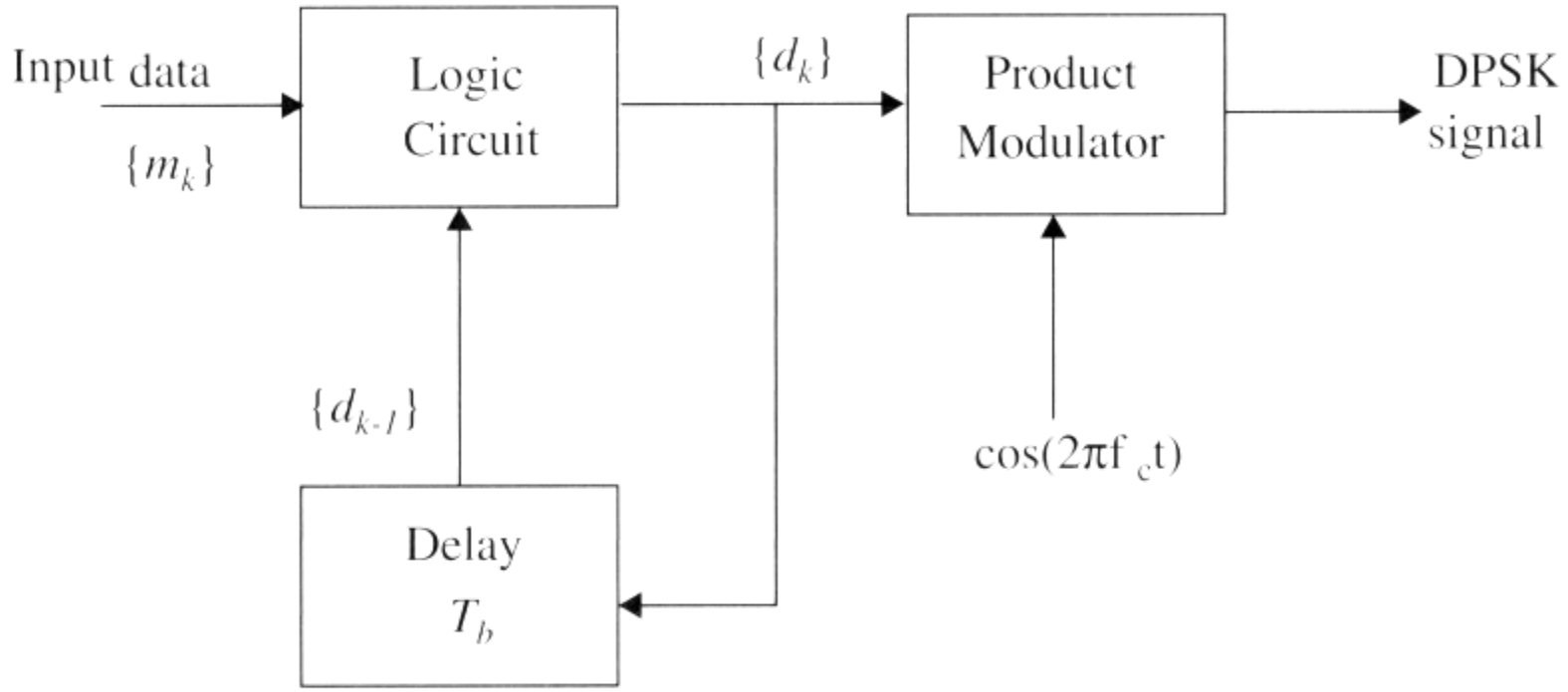

Figure 6.24 Block diagram of a DPSK transmitter.

DPSK receiver

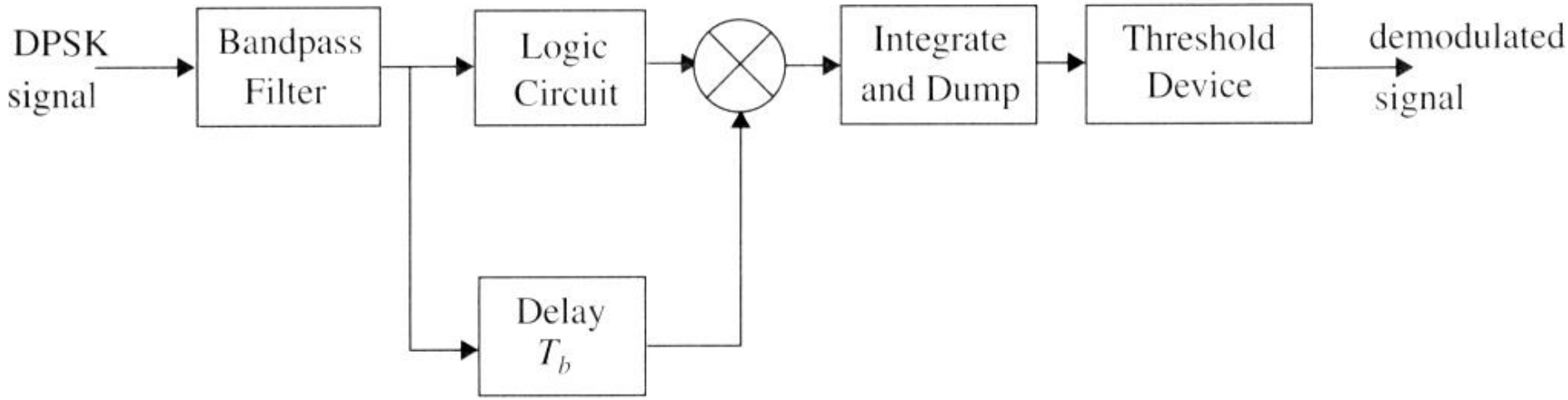

Figure 6.25 Block diagram of DPSK receiver.

QPSK constellation diagrams

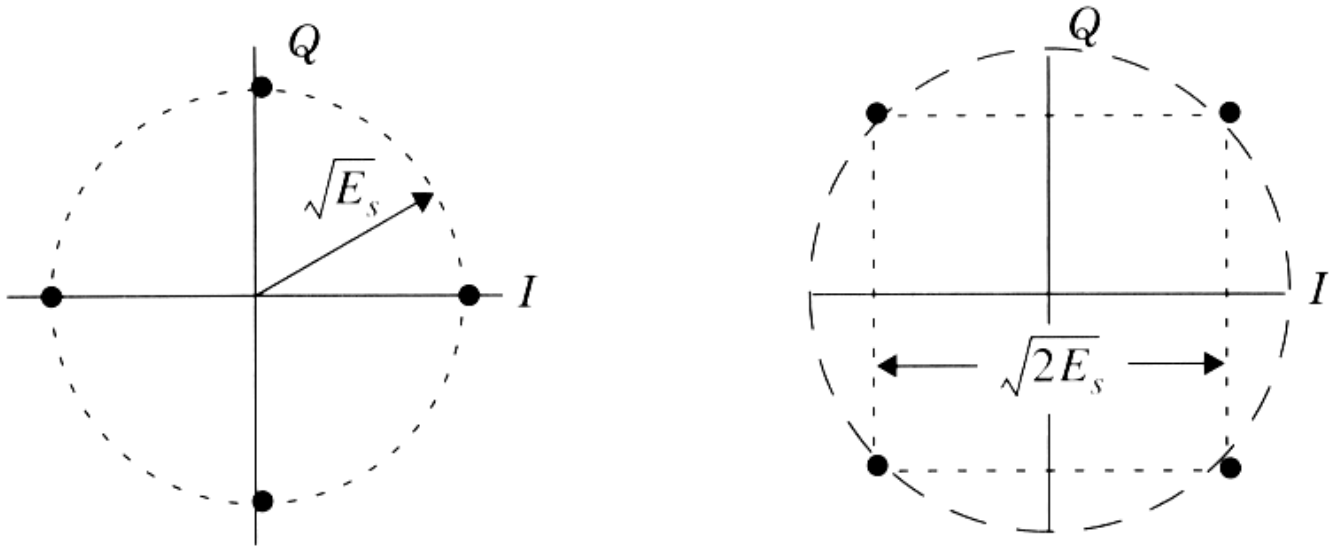

Figure 6.26 (a) QPSK constellation where the carrier phases are 0, π/2, π, 3π/2; (b) QPSK constellation where the carrier phases are π/4, 3π/4, 5π/4, 7π/4.

Virtues of Pulse Shaping

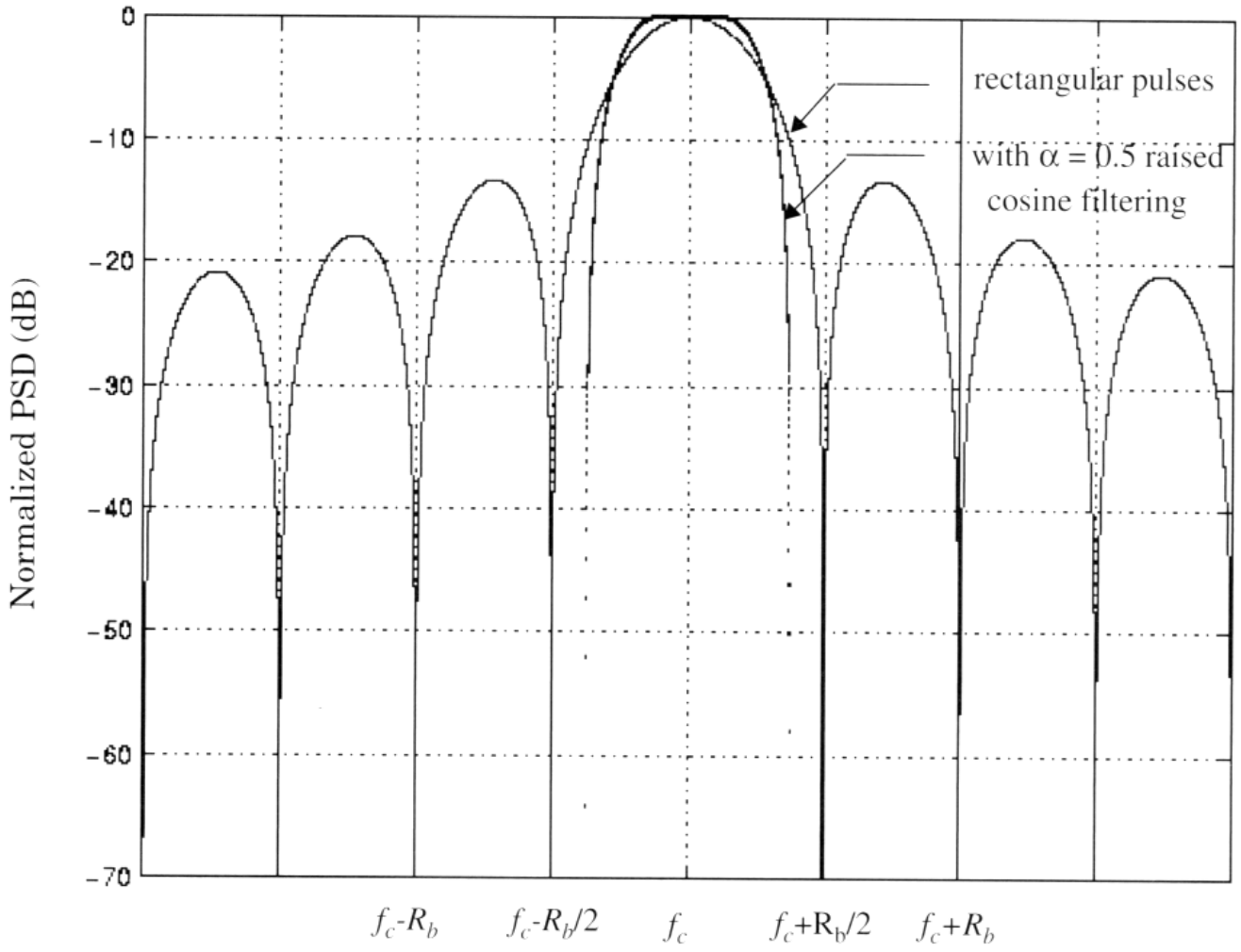

Figure 6.27 Power spectral density of a QPSK signal.

QPSK modulation

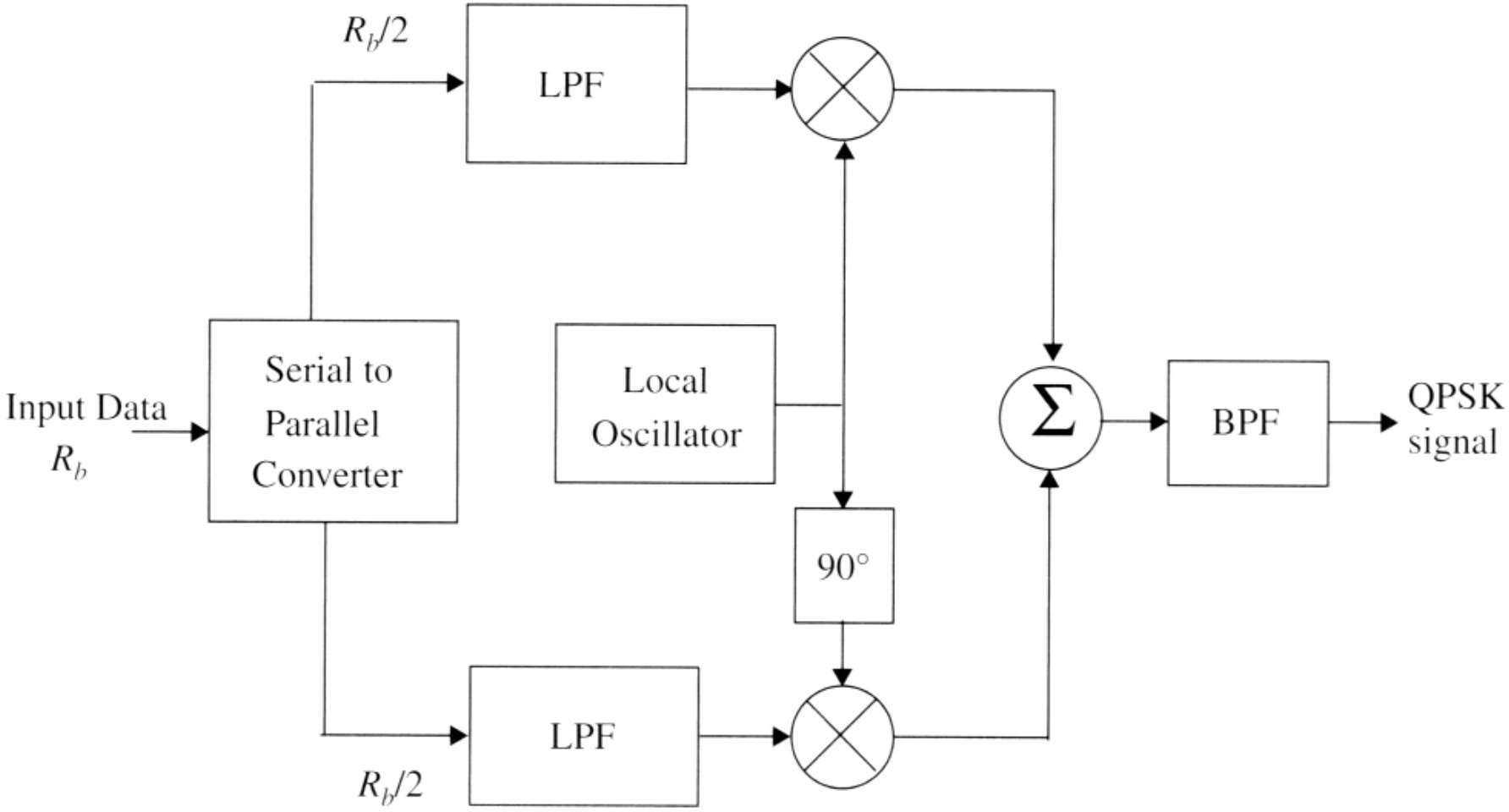

Figure 6.28 Block diagram of a QPSK transmitter.

QPSK receiver

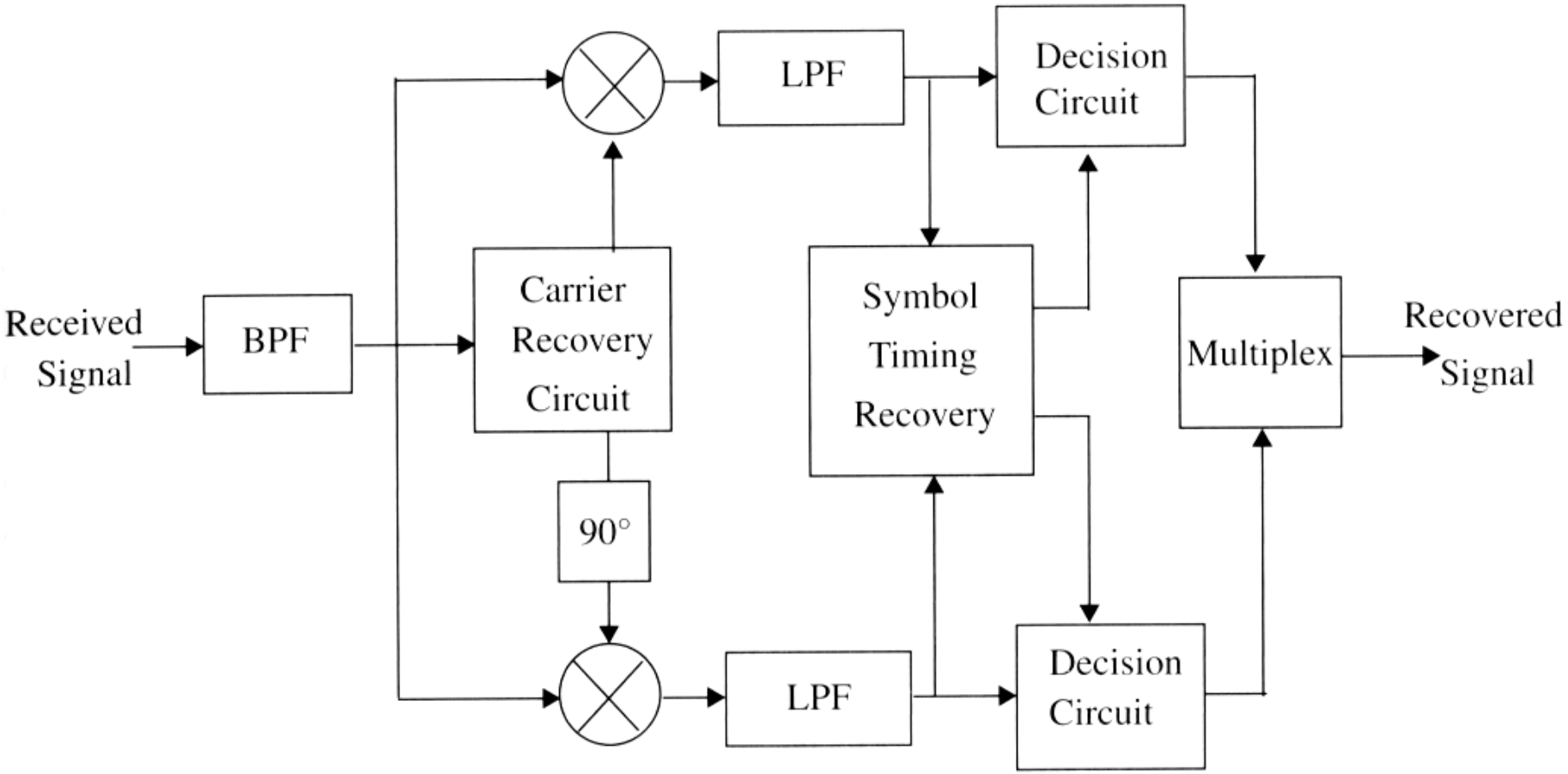

Figure 6.29 Block diagram of a QPSK receiver.

Offset QPSK waveforms

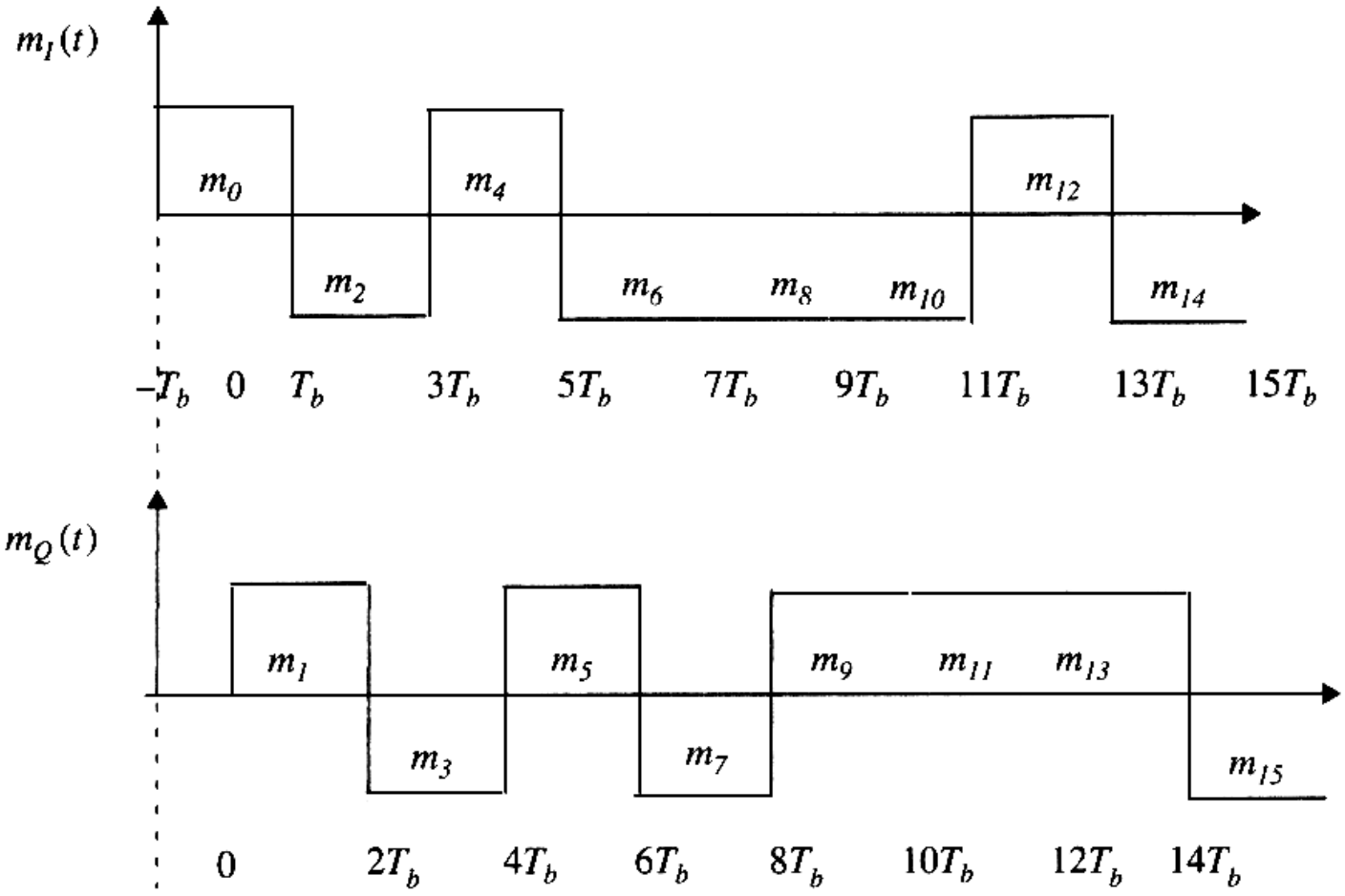

Figure 6.30 The time offset waveforms that are applied to the in-phase and quadrature arms of an OQPSK modulator. Notice that a half-symbol offset is used.

Pi/4 QPSK signaling

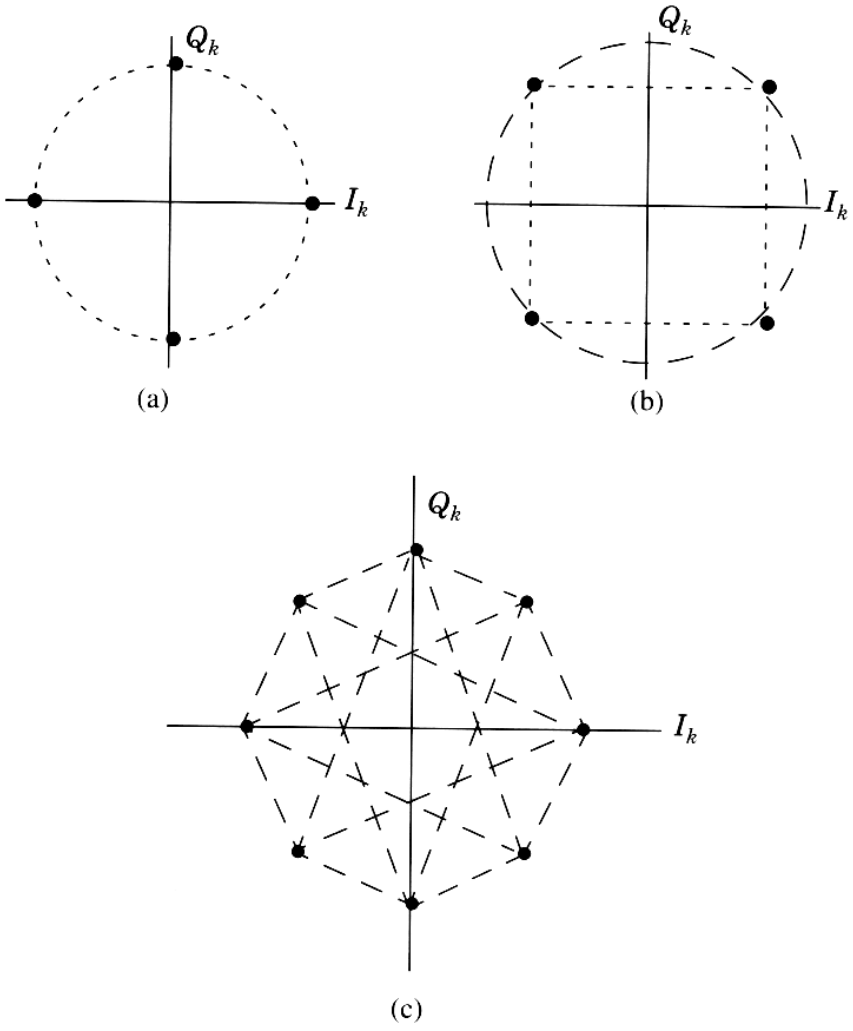

Figure 6.31 Constellation diagram of a $\pi/4$ QPSK signal: (a) possible states for θ_k when $\theta_{k-1} = n\pi/4$; (b) possible states when $\theta_{k-1} = n\pi/2$; (c) all possible states.

Pi/4 QPSK phase shifts

Table 6.2 Carrier Phase Shifts Corresponding to Various Input Bit Pairs [Feh91], [Rap91b]

Information bits m_{Ik}, m_{Qk}	Phase shift ϕ_k
1 1	$\pi/4$
0 1	$3\pi/4$
0 0	$-3\pi/4$
1 0	$-\pi/4$

Pi/4 QPSK transmitter

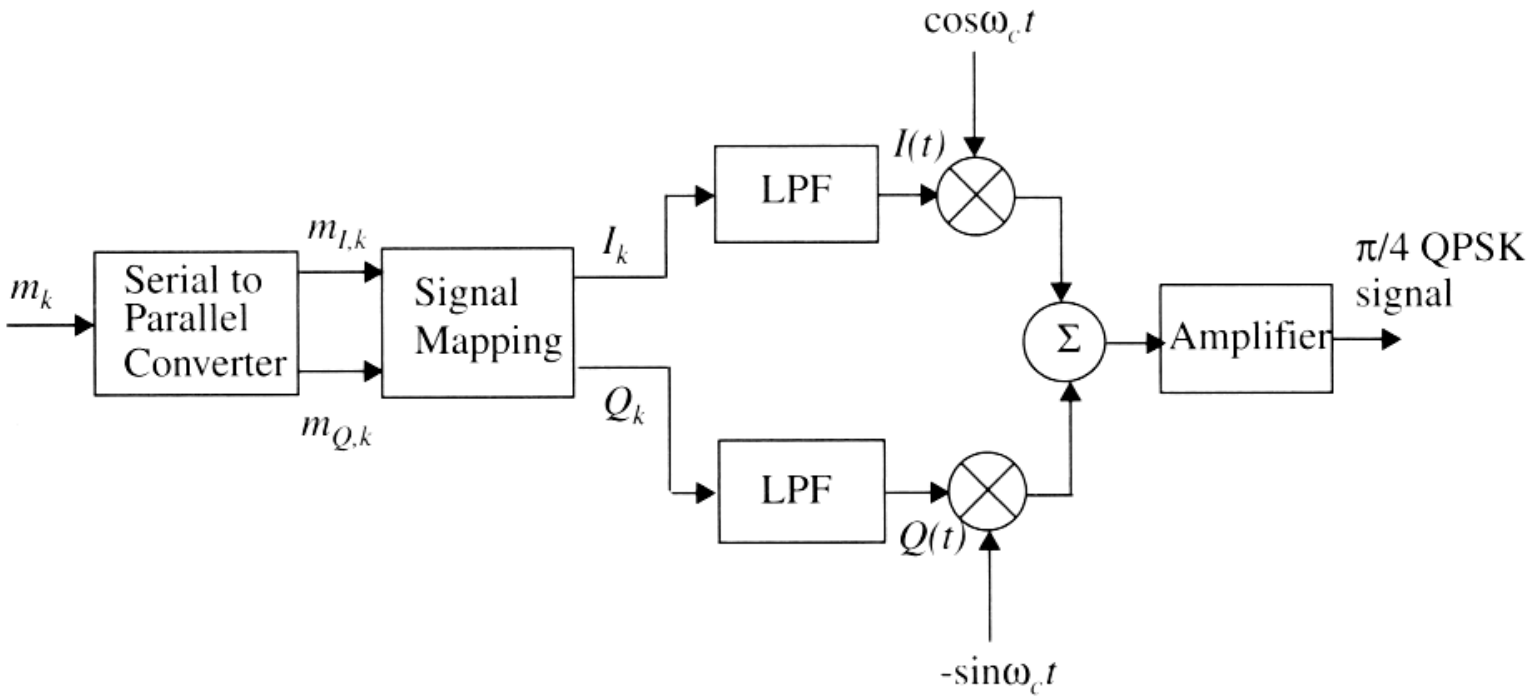

Figure 6.32 Generic π/4 QPSK transmitter.

Differential detection of pi/4 QPSK

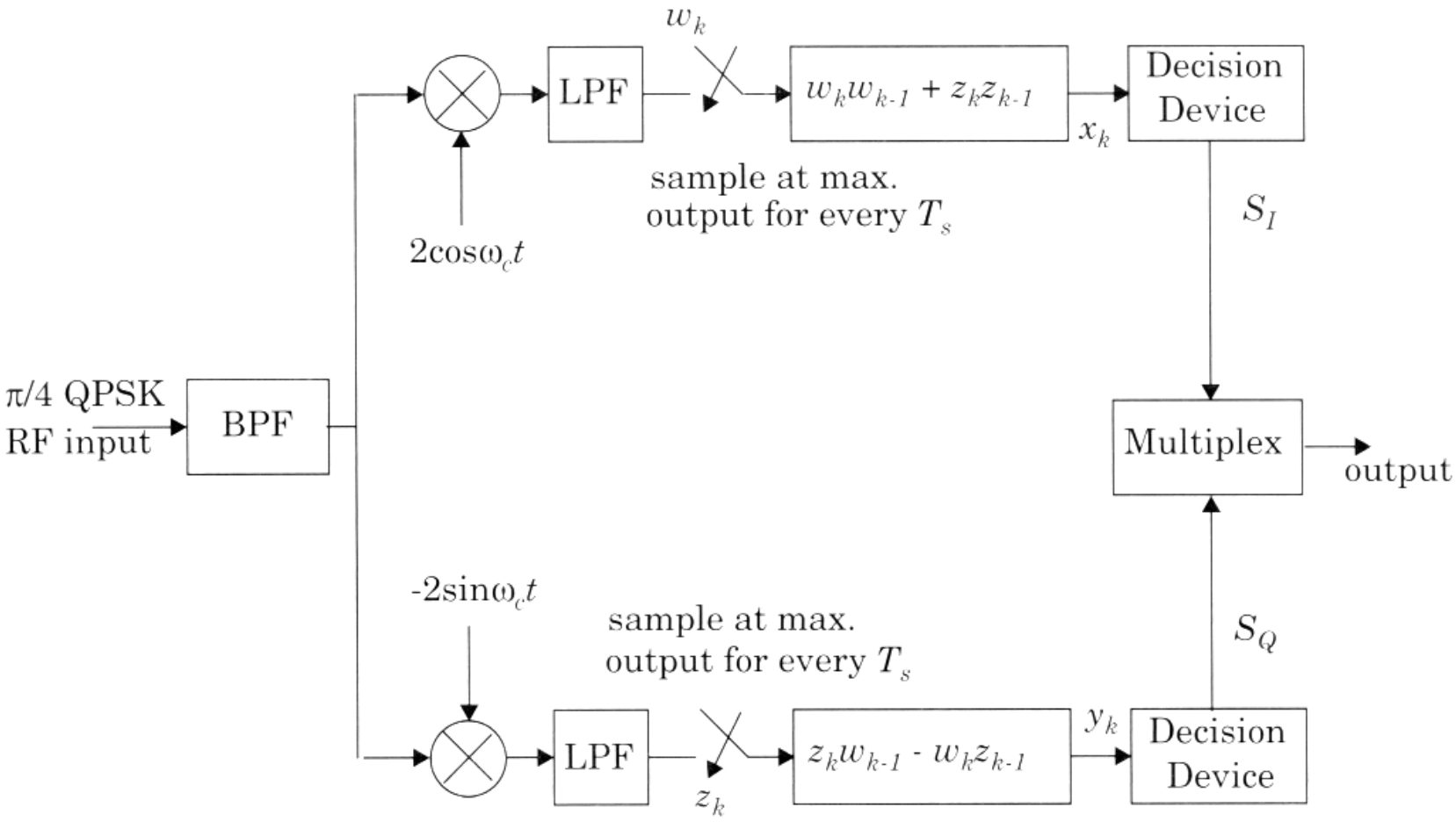

Figure 6.33 Block diagram of a baseband differential detector [from [Feh91] © IEEE].

IF Differential Detection

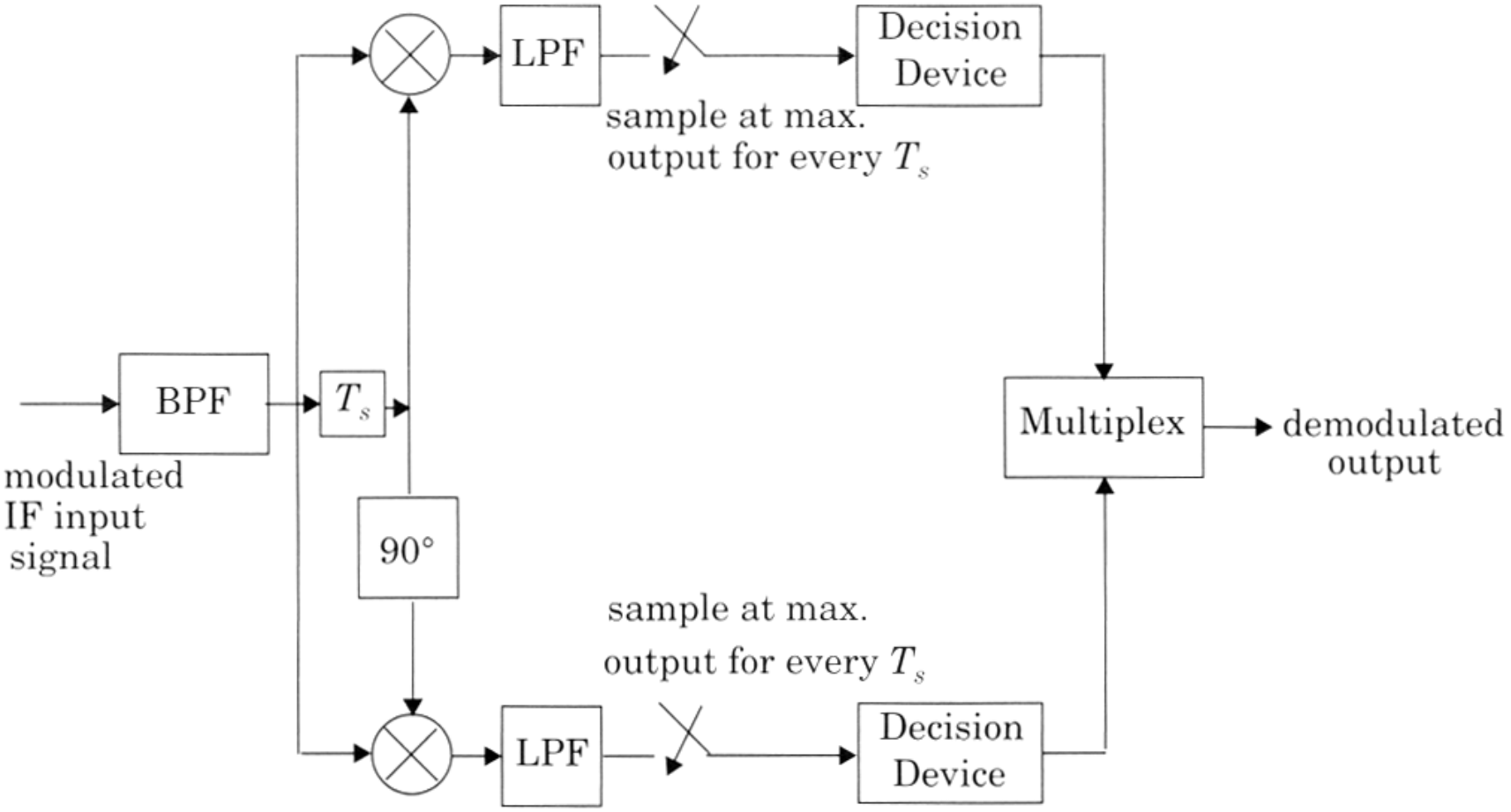

Figure 6.34 Block diagram of an IF differential detector for π/4 QPSK.

FM Discriminator detector

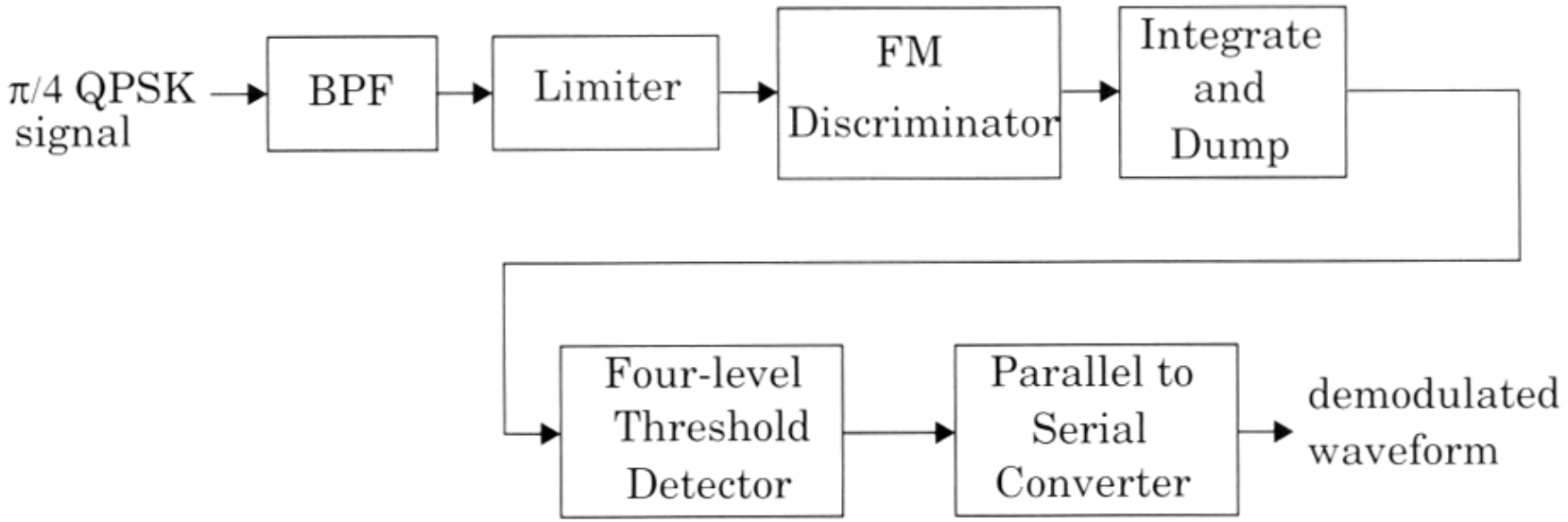

Figure 6.35 FM discriminator detector for π/4 DQPSK demodulation.

FSK Coherent Detection

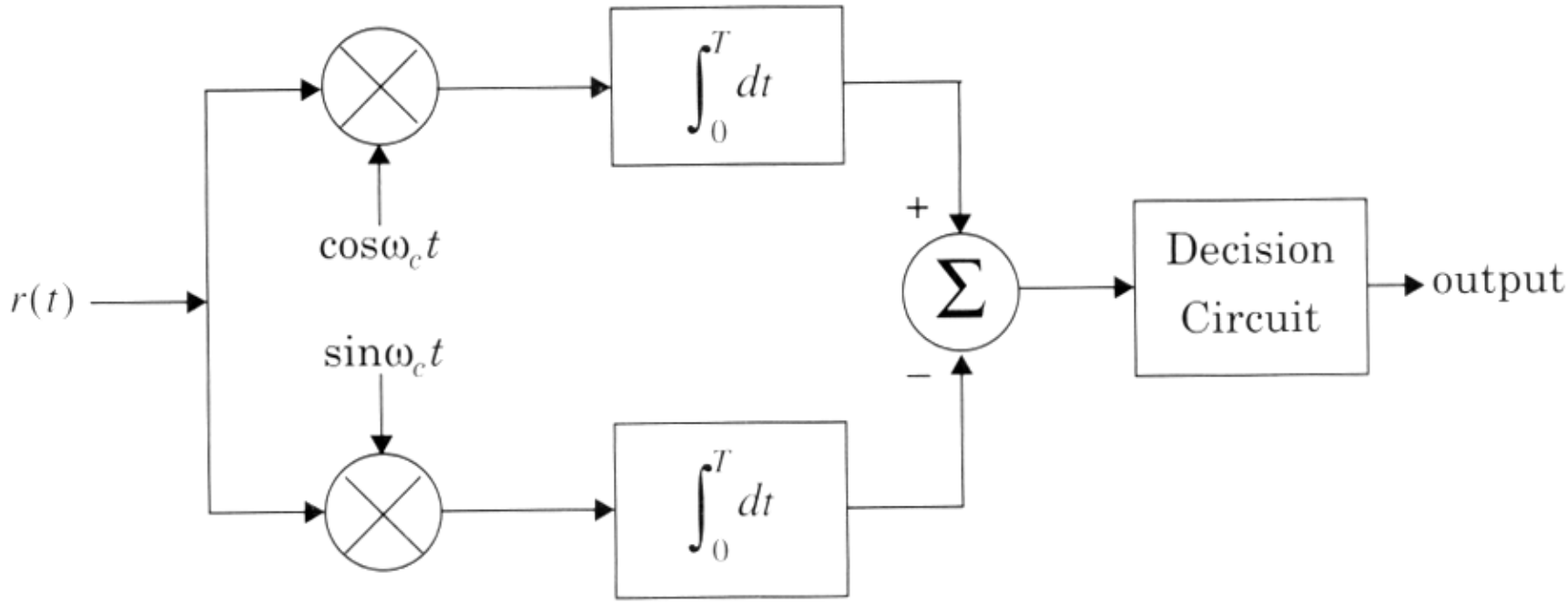

Figure 6.36 Coherent detection of FSK signals.

Noncoherent FSK

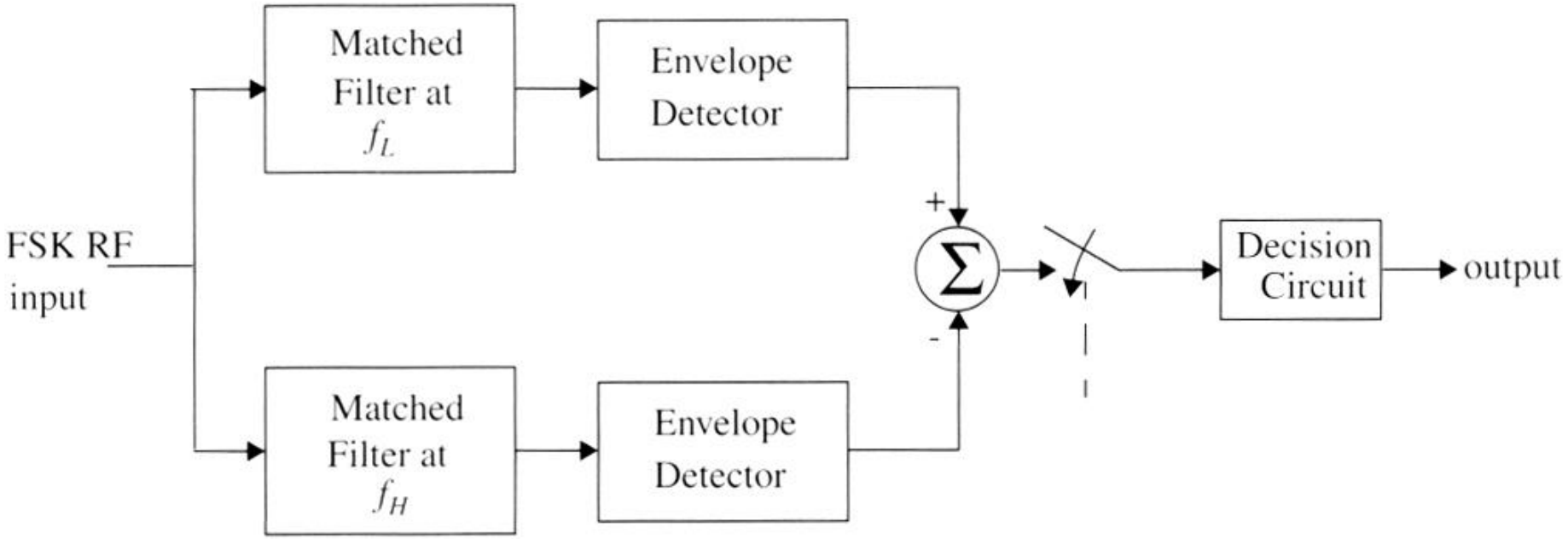

Figure 6.37 Block diagram of noncoherent FSK receiver.

Minimum Shift Keying spectra

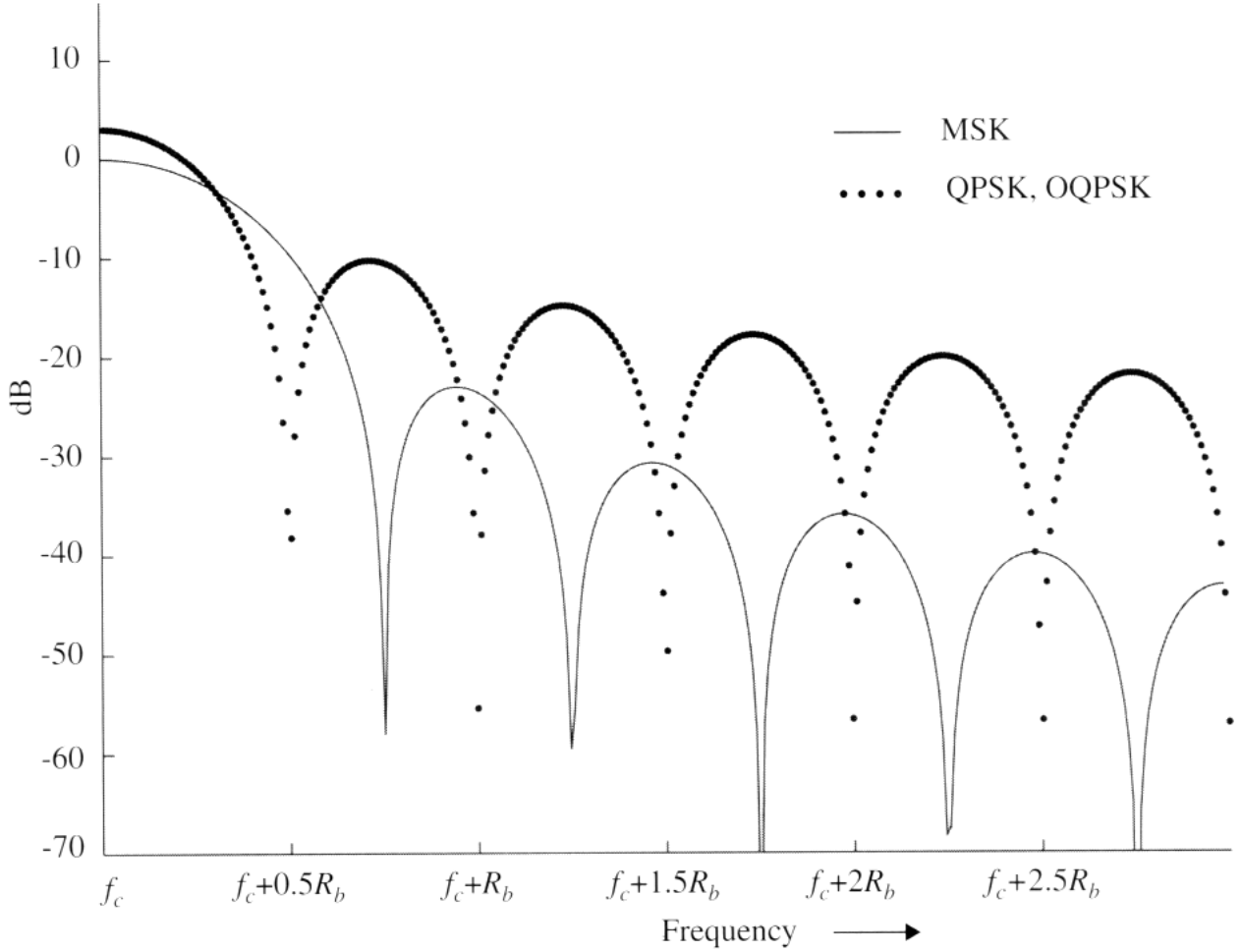

Figure 6.38 Power spectral density of MSK signals as compared to QPSK and OQPSK signals.

MSK modulation

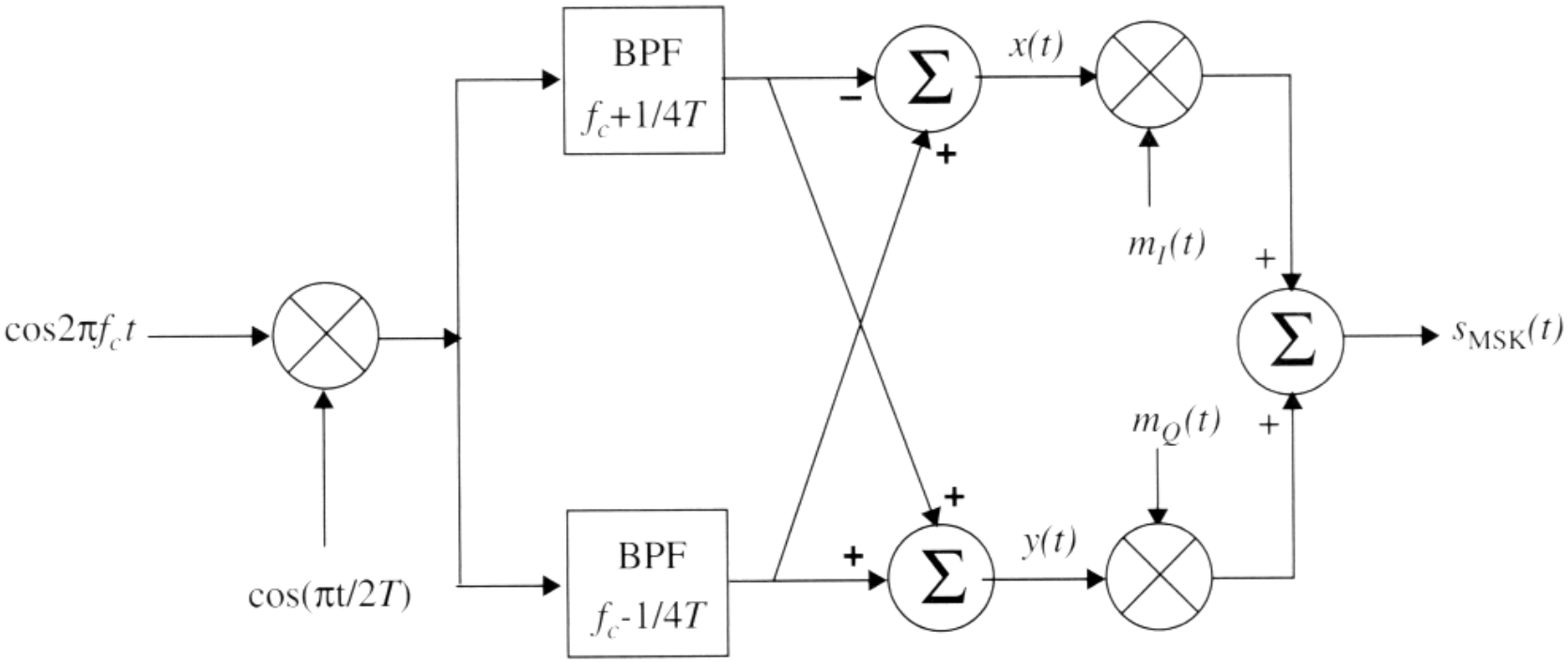

Figure 6.39 Block diagram of an MSK transmitter. Note that $m_I(t)$ and $m_Q(t)$ are offset by T_b.

MSK reception

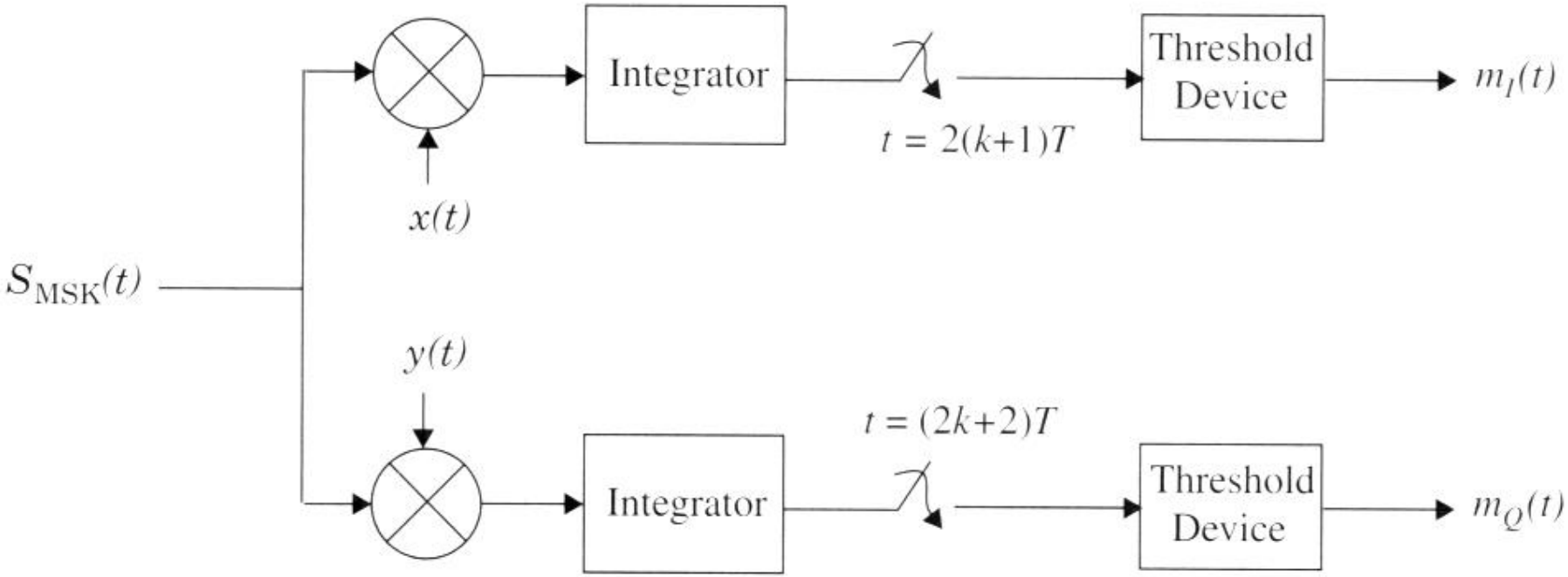

Figure 6.40 Block diagram of an MSK receiver.

GMSK spectral shaping

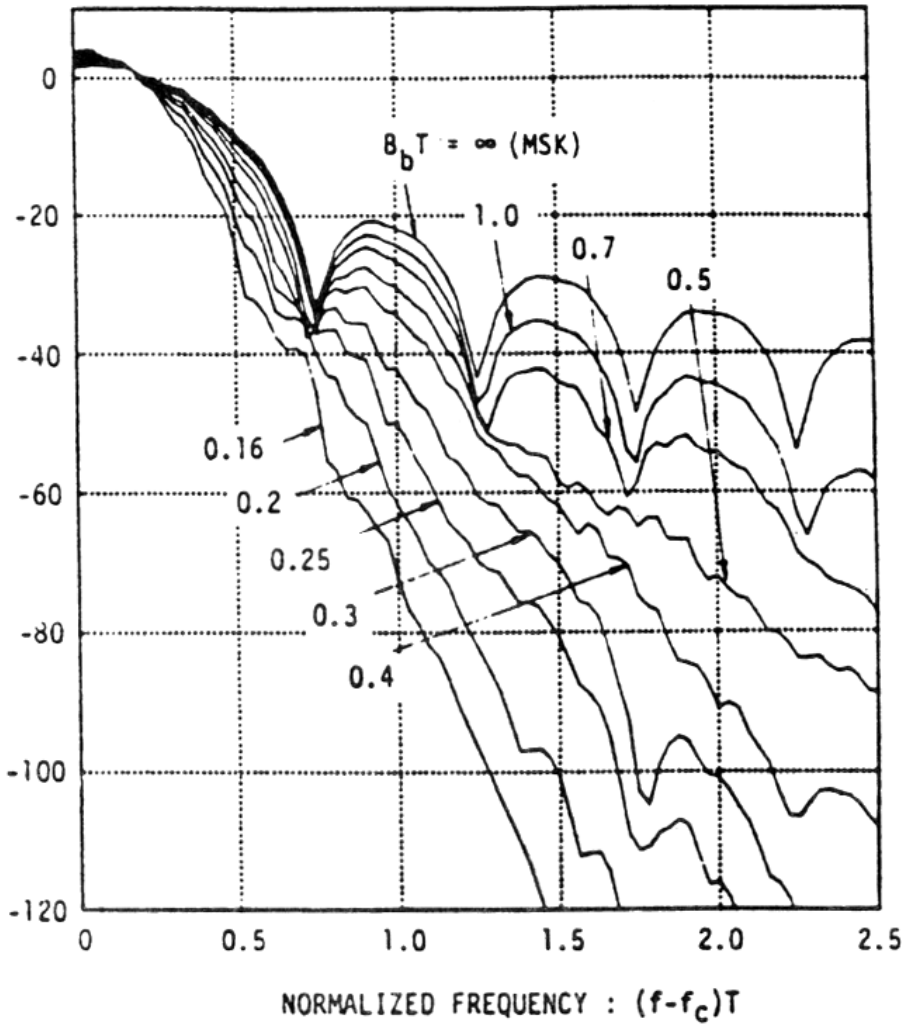

Figure 6.41 Power spectral density of a GMSK signal [from [Mur81] © IEEE].

GMSK spectra shaping

Table 6.3 Occupied RF Bandwidth (for GMSK and MSK as a fraction of R_b) Containing a Given Percentage of Power [Mur81]. Notice that GMSK is Spectrally Tighter than MSK

BT	90%	99%	99.9%	99.99%
0.2 GMSK	0.52	0.79	0.99	1.22
0.25 GMSK	0.57	0.86	1.09	1.37
0.5 GMSK	0.69	1.04	1.33	2.08
MSK	0.78	1.20	2.76	6.00

Simple GMSK generation

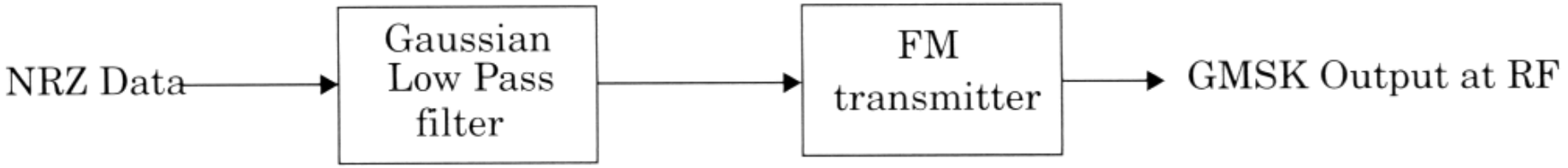

Figure 6.42 Block diagram of a GMSK transmitter using direct FM generation.

GMSK Demodulator

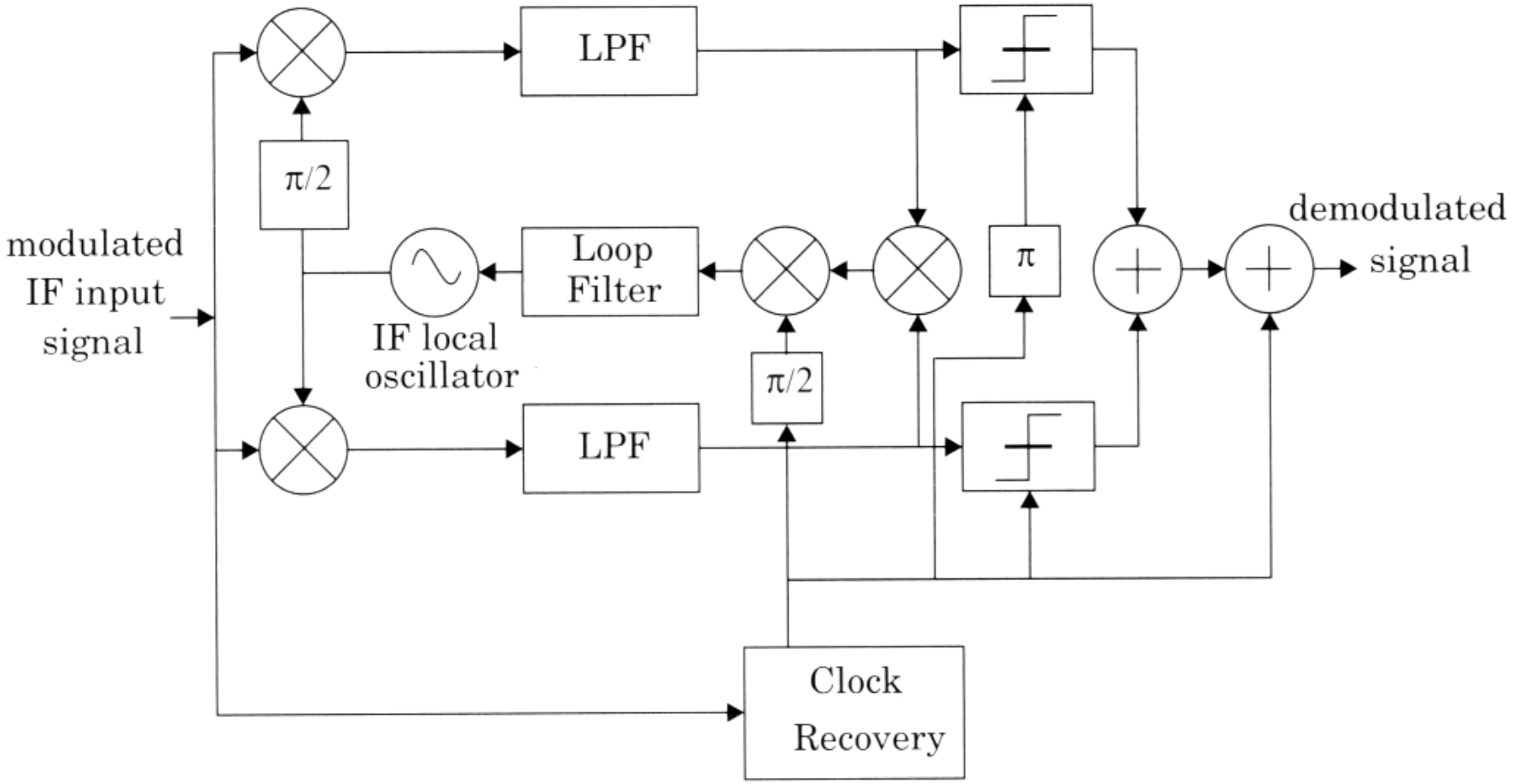

Figure 6.43 Block diagram of a GMSK receiver.

Digital GMSK demodulator

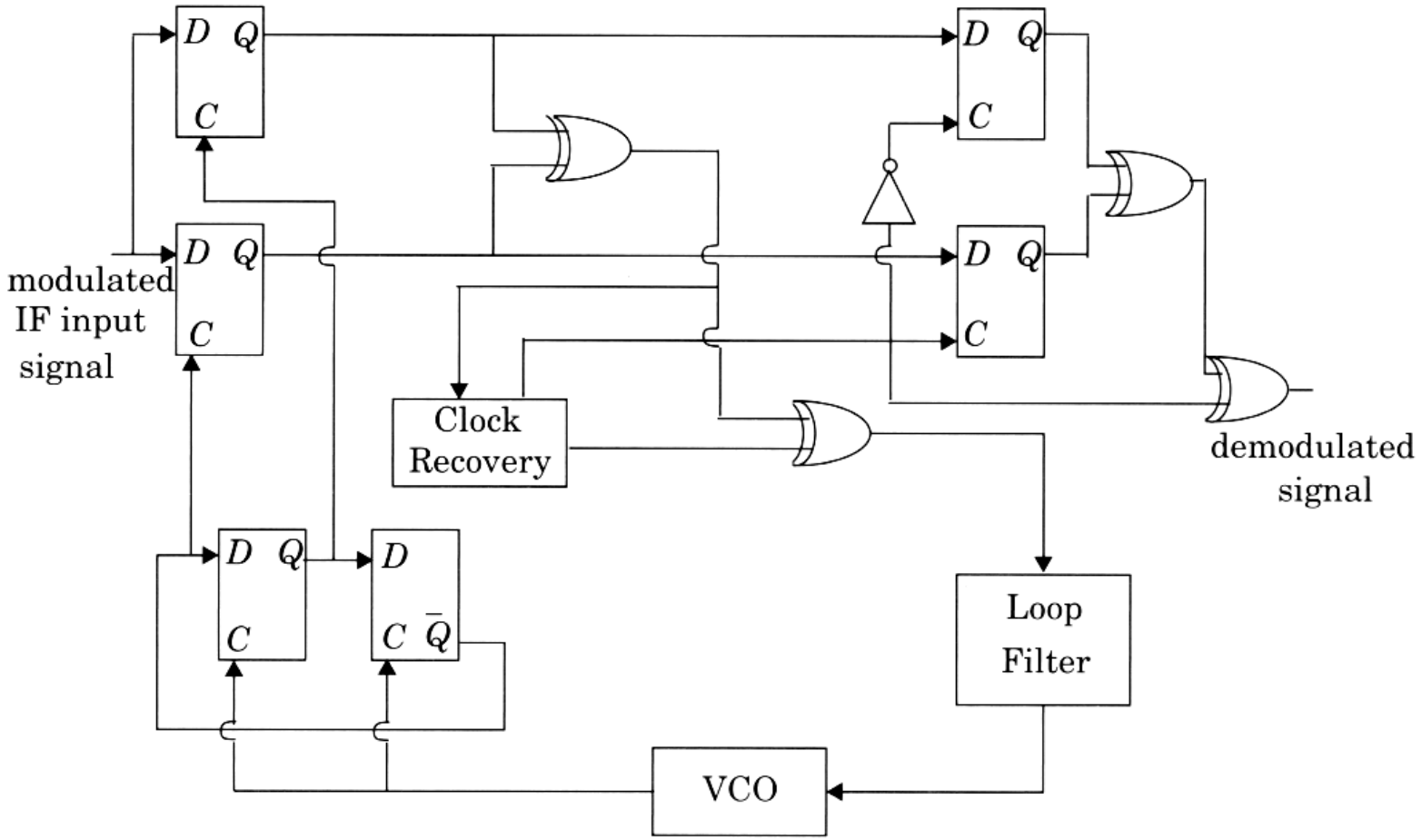

Figure 6.44 Digital logic circuit for GMSK demodulation [from [deB72] © IEEE].

8-PSK Signal Constellation

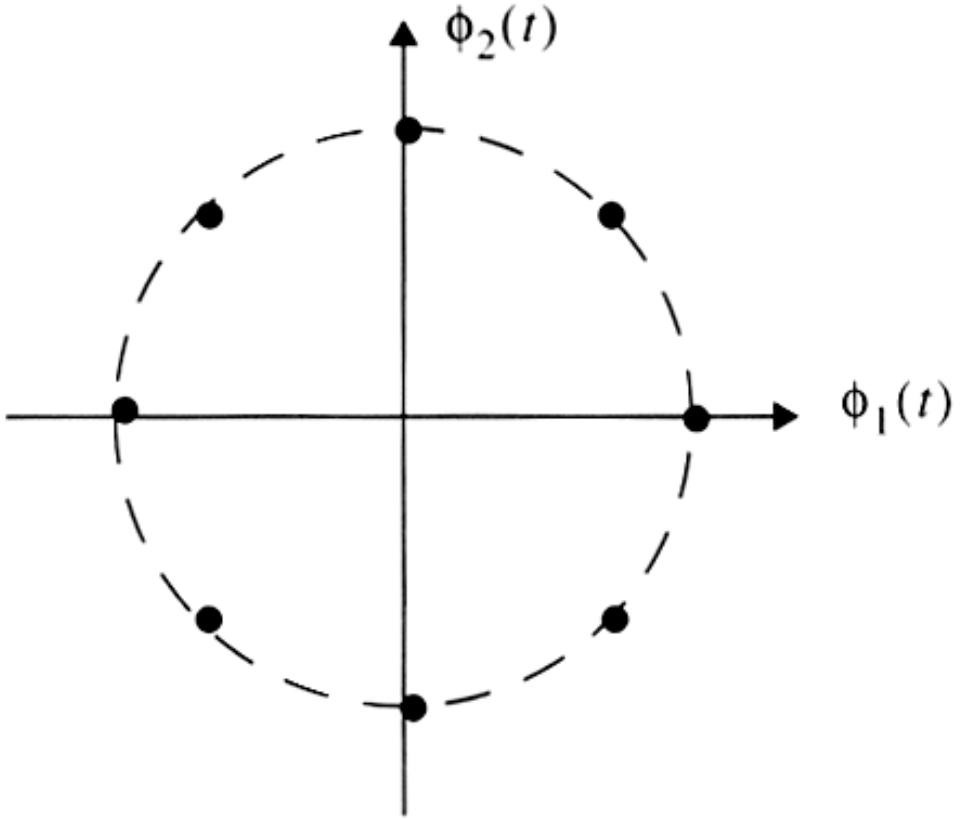

Figure 6.45 Constellation diagram of an M-ary PSK system ($M = 8$).

Bandwidth vs. Power Efficiency

Table 6.4 Bandwidth and Power Efficiency of M-ary PSK Signals

M	2	4	8	16	32	64
$\eta_B = R_b/B^*$	0.5	1	1.5	2	2.5	3
E_b/N_o for BER=10^{-6}	10.5	10.5	14	18.5	23.4	28.5

* B: First null bandwidth of M-ary PSK signals

Pulse Shaped M-PSK

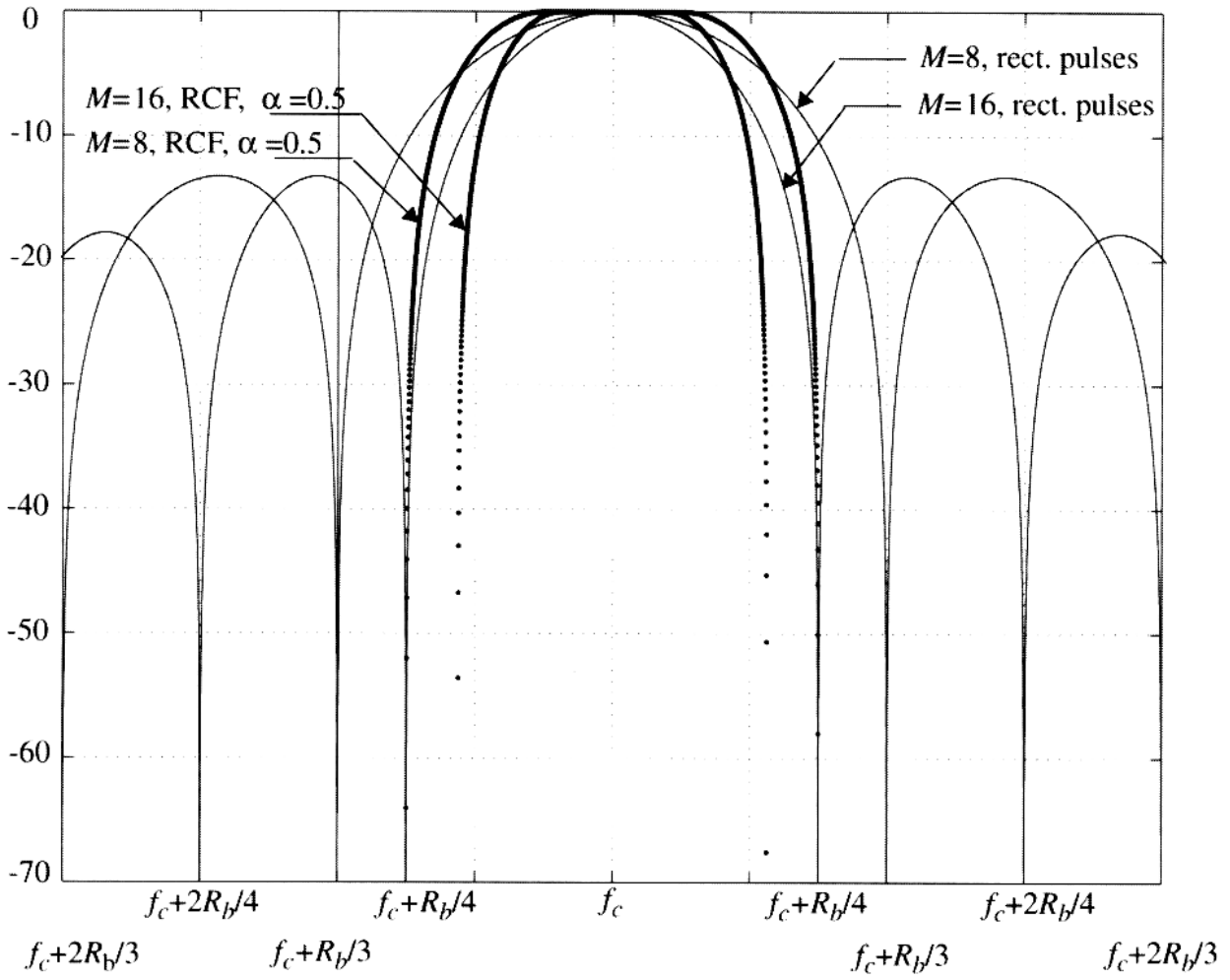

Figure 6.46 M-ary PSK power spectral density, for M = 8, 16 (PSD for both rectangular and raised cosine filtered pulses are shown for fixed R_b).

16-QAM Signal Constellation

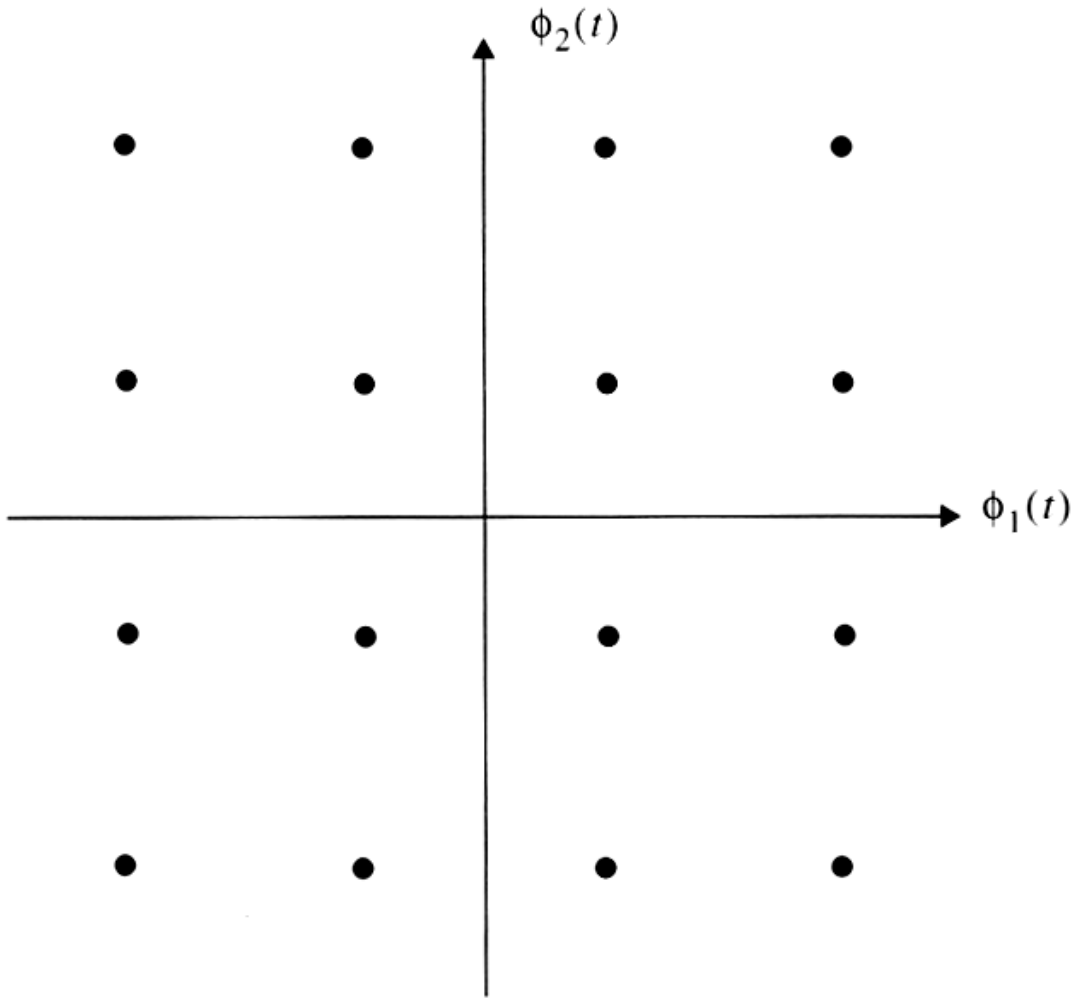

Figure 6.47 Constellation diagram of an M-ary QAM ($M = 16$) signal set.

QAM efficiencies

Table 6.5 Bandwidth and Power Efficiency of QAM [Zie92]

M	4	16	64	256	1024	4096
η_B	1	2	3	4	5	6
E_b/N_o for BER = 10^{-6}	10.5	15	18.5	24	28	33.5

M-ary FSK efficiencies

Table 6.6 Bandwidth and Power Efficiency of Coherent M-ary FSK [Zie92]

M	2	4	8	16	32	64
η_B	0.4	0.57	0.55	0.42	0.29	0.18
E_b/N_o for BER = 10^{-6}	13.5	10.8	9.3	8.2	7.5	6.9

PN Sequence Generator

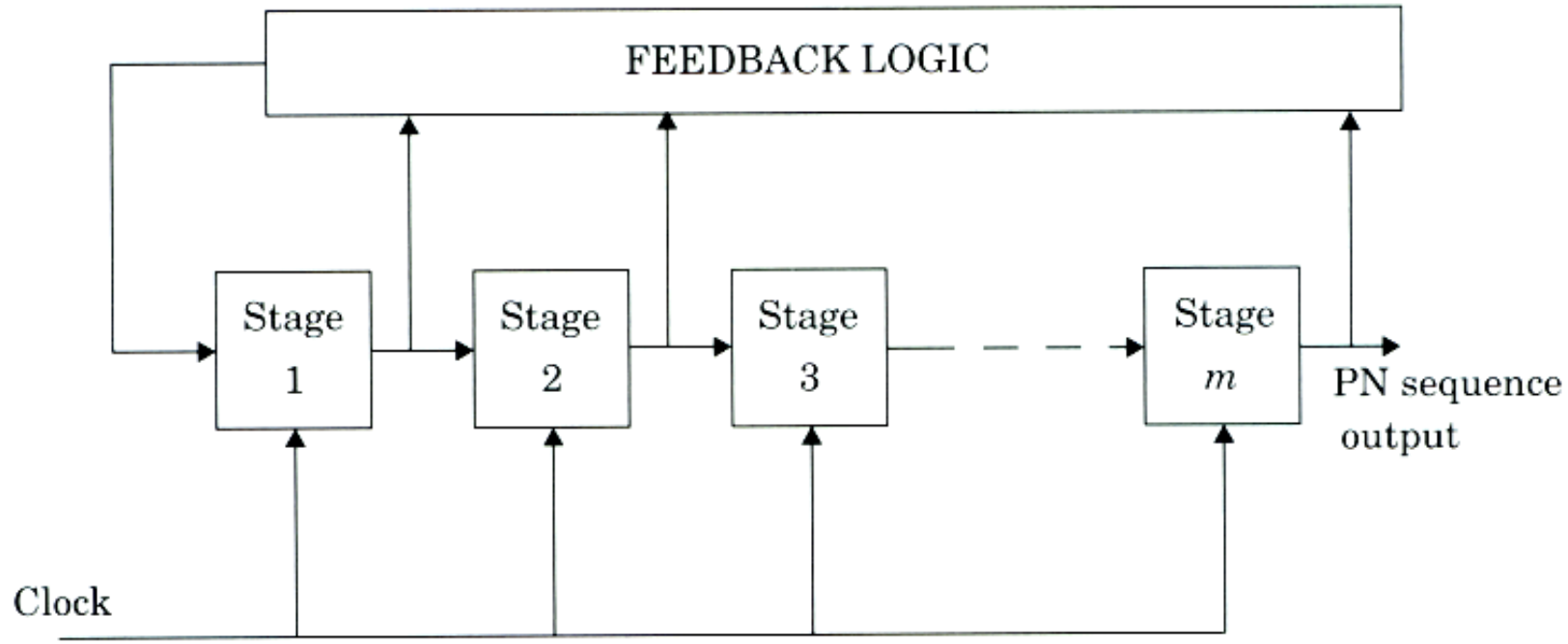

Figure 6.48 Block diagram of a generalized feedback shift register with *m* stages.

Direct Sequence Spread Spectrum

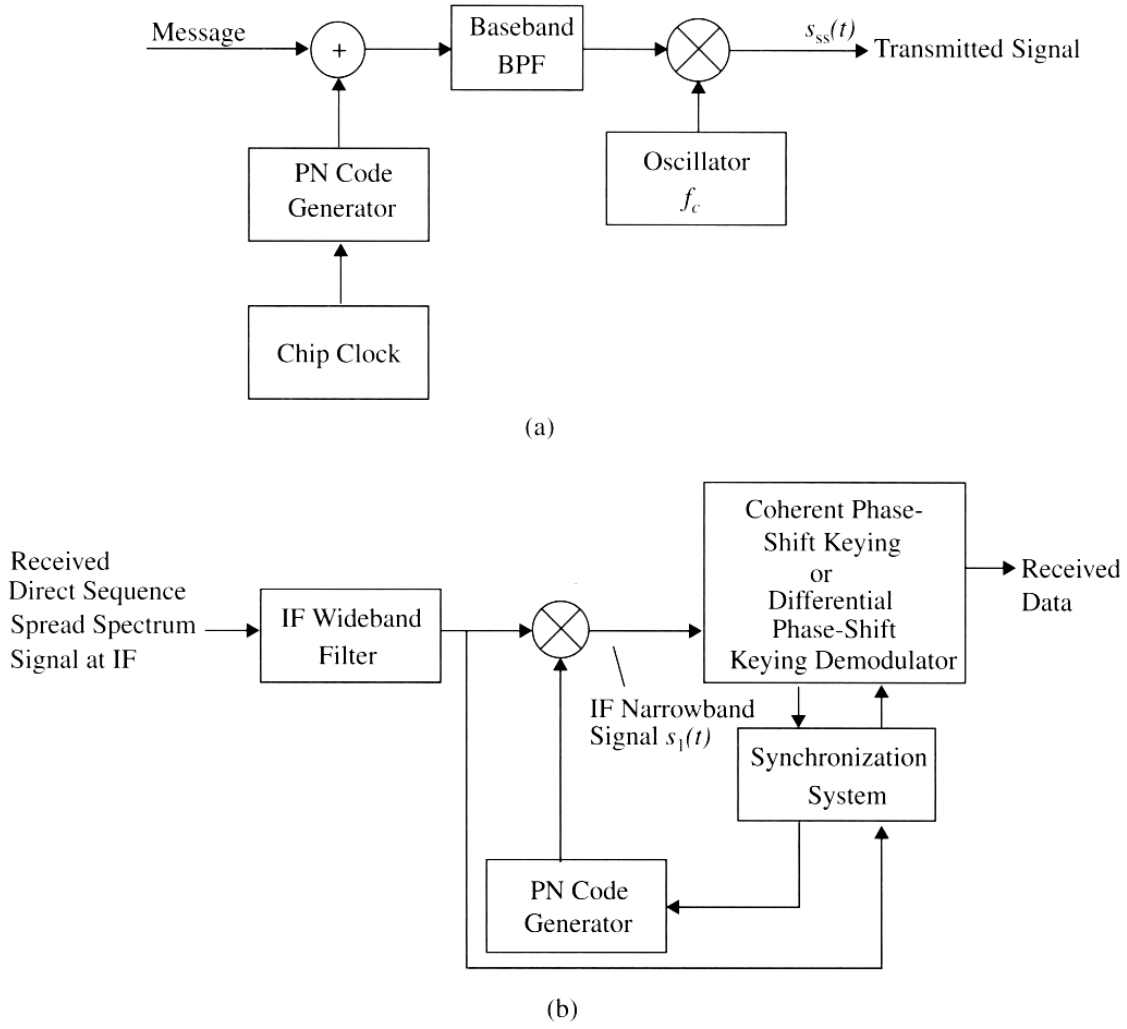

Figure 6.49 Block diagram of a DS–SS system with binary phase modulation: (a) transmitter; and (b) receiver.

Direct Sequence Spreading

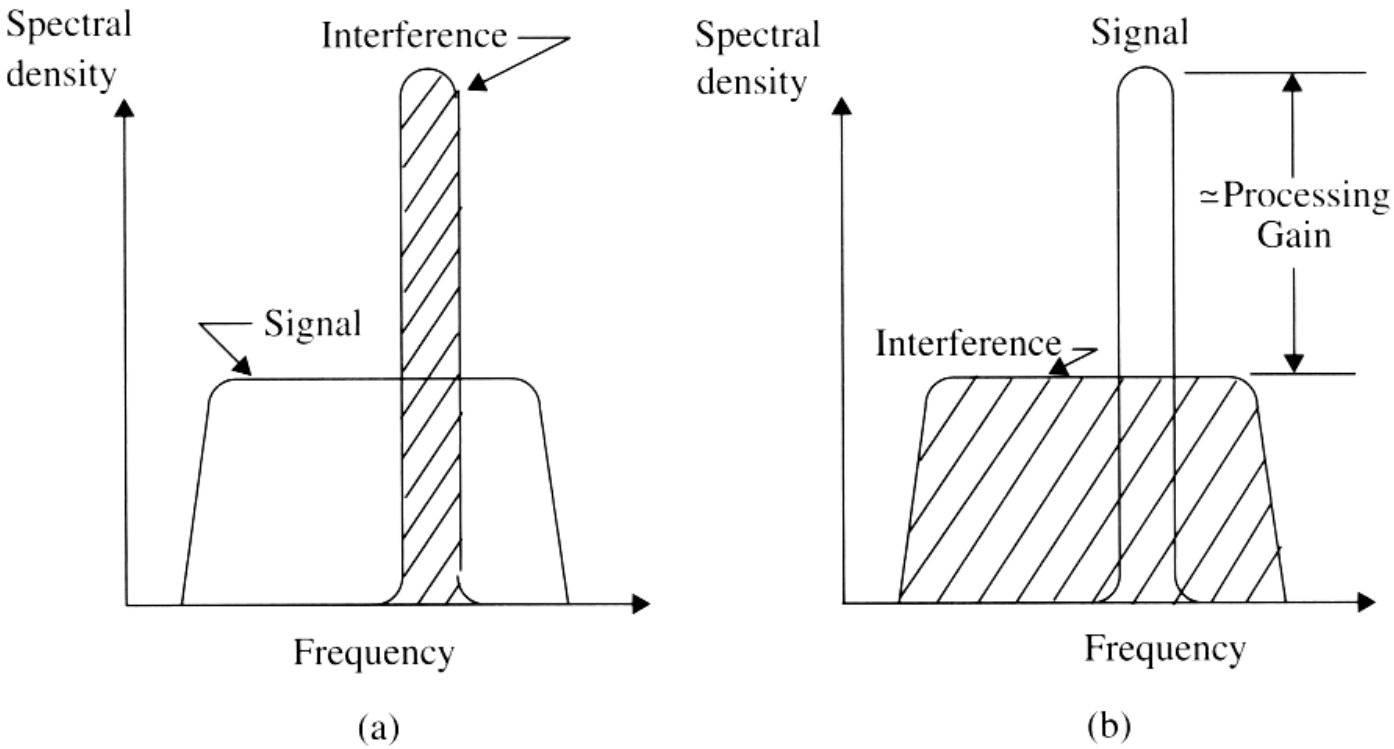

Figure 6.50 Spectra of desired received signal with interference: (a) wideband filter output and (b) correlator output after despreading.

Frequency Hopping Spread Spectrum

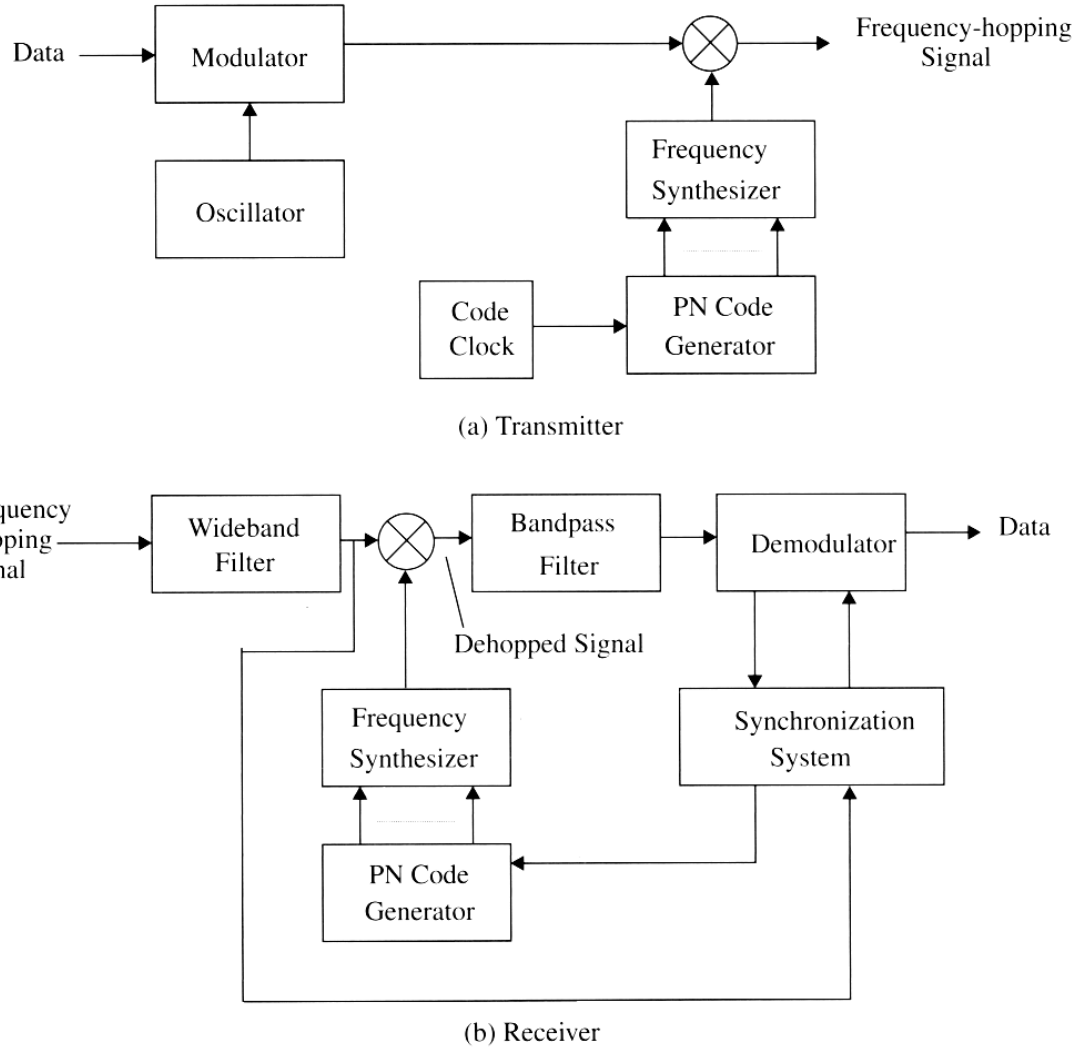

Figure 6.51 Block diagram of frequency hopping (FH) system with single channel modulation.

CDMA – Multiple Users

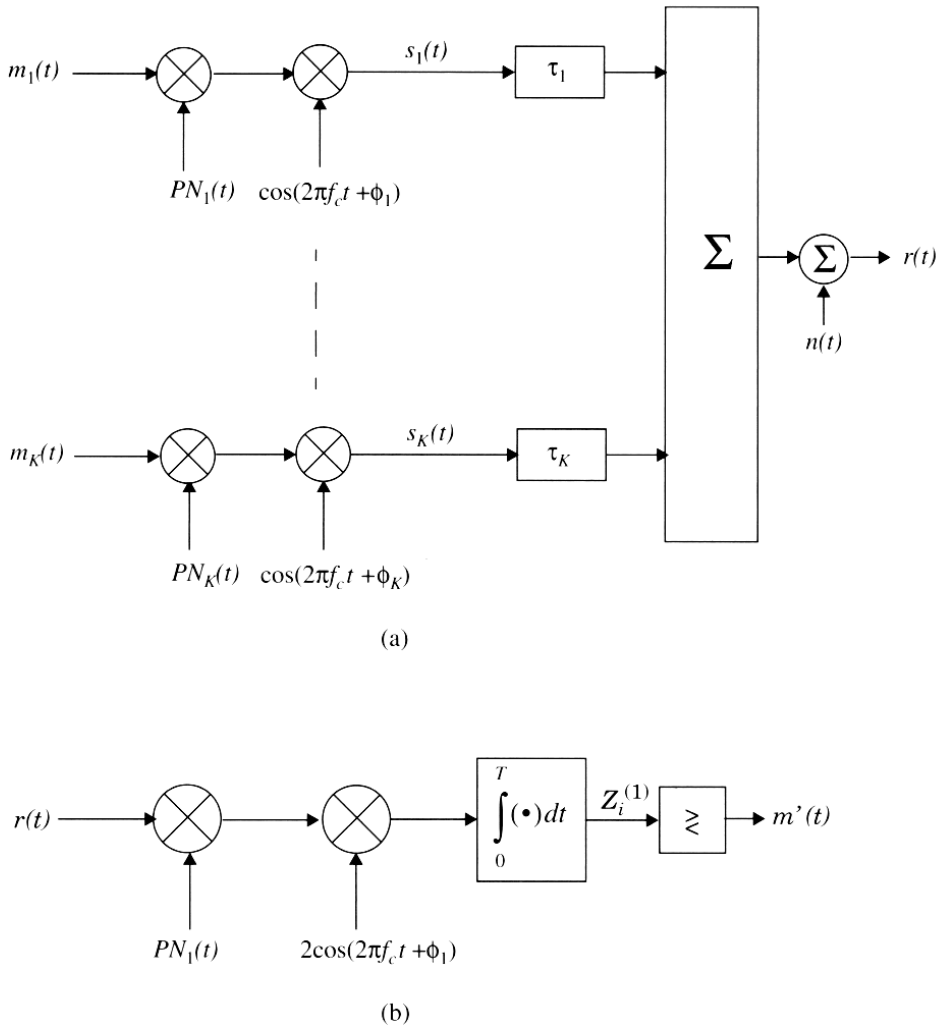

Figure 6.52 A simplified diagram of a DS–SS system with *K* users. (a) Model of *K* users in a CDMA spread spectrum system; (b) receiver structure for User 1.

Effects of Fading

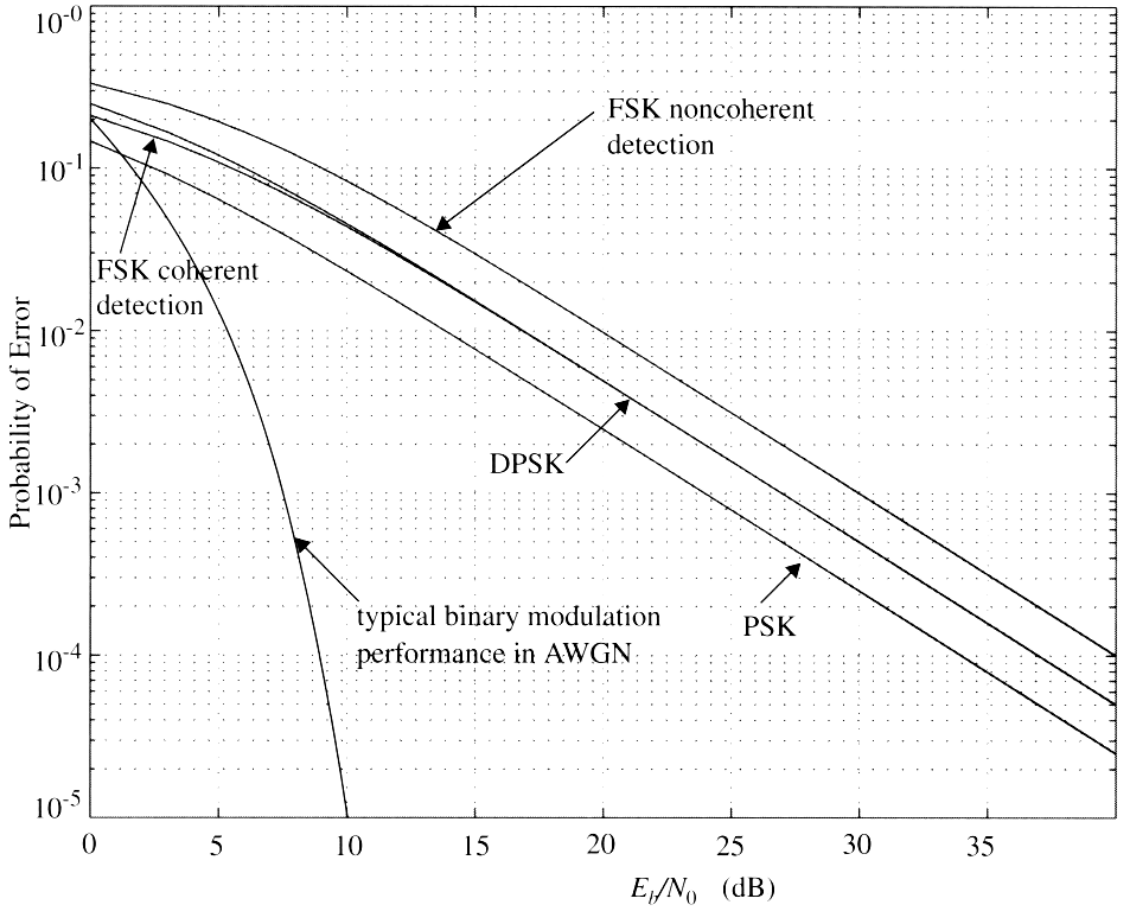

Figure 6.53 Bit error rate performance of binary modulation schemes in a Rayleigh flat-fading channel as compared to a typical performance curve in AWGN.

Irreducible Bit Error Rate due to multipath

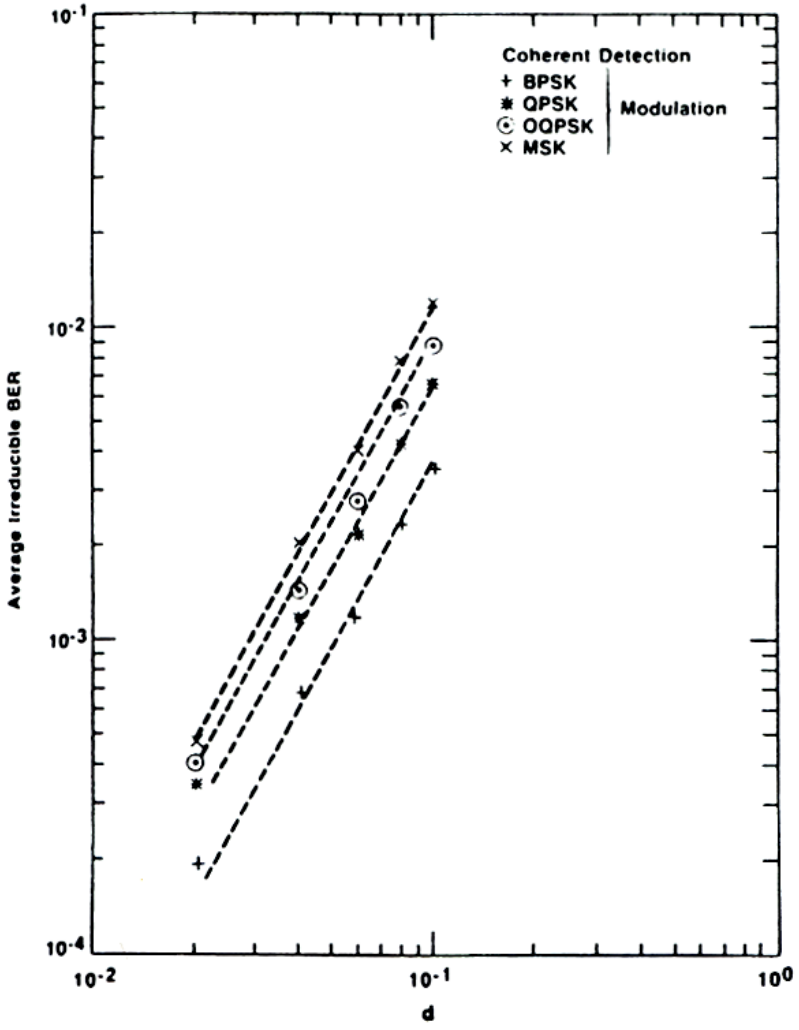

Figure 6.54 The irreducible BER performance for different modulations with coherent detection for a channel with a Gaussian shaped power delay profile. The parameter d is the rms delay spread normalized by the symbol period [from [Chu87] © IEEE].

Irreducible Bit Error Rate due to multipath

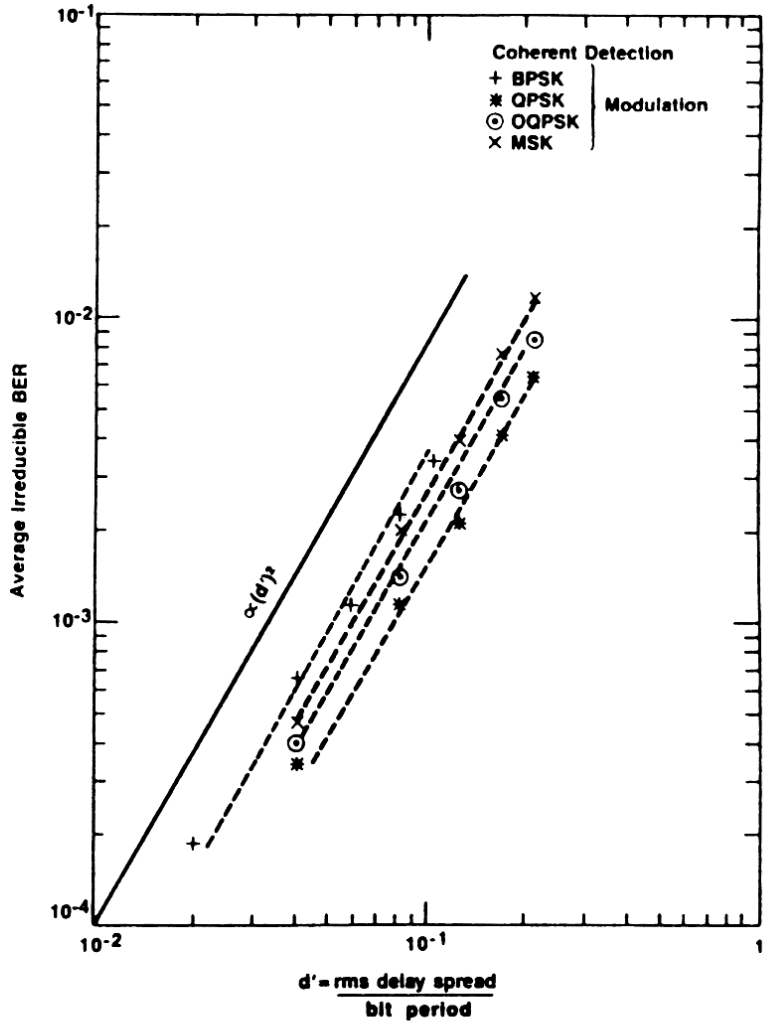

Figure 6.55 The same set of curves as plotted in Figure 6.54 plotted as a function of rms delay spread normalized by bit period [from [Chu87] © IEEE].

Simulation of Fading and Multipath

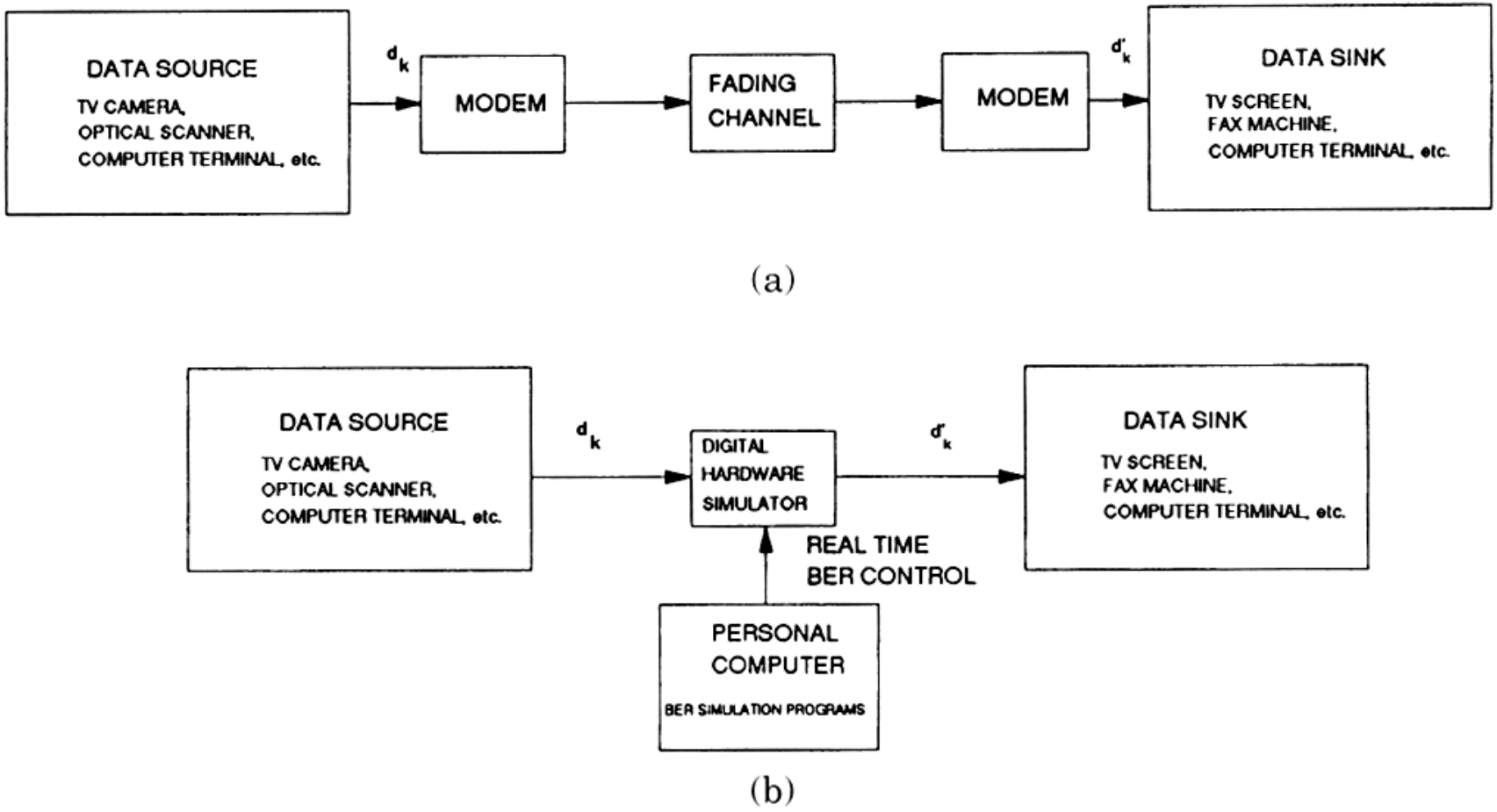

Figure 6.56 The BERSIM concept: (a) Block diagram of actual digital communication system; (b) block diagram of BERSIM using a baseband digital hardware simulator with software simulation as a driver for real-time BER control (US Patent 5,233,628).

Irreducible BER due to fading

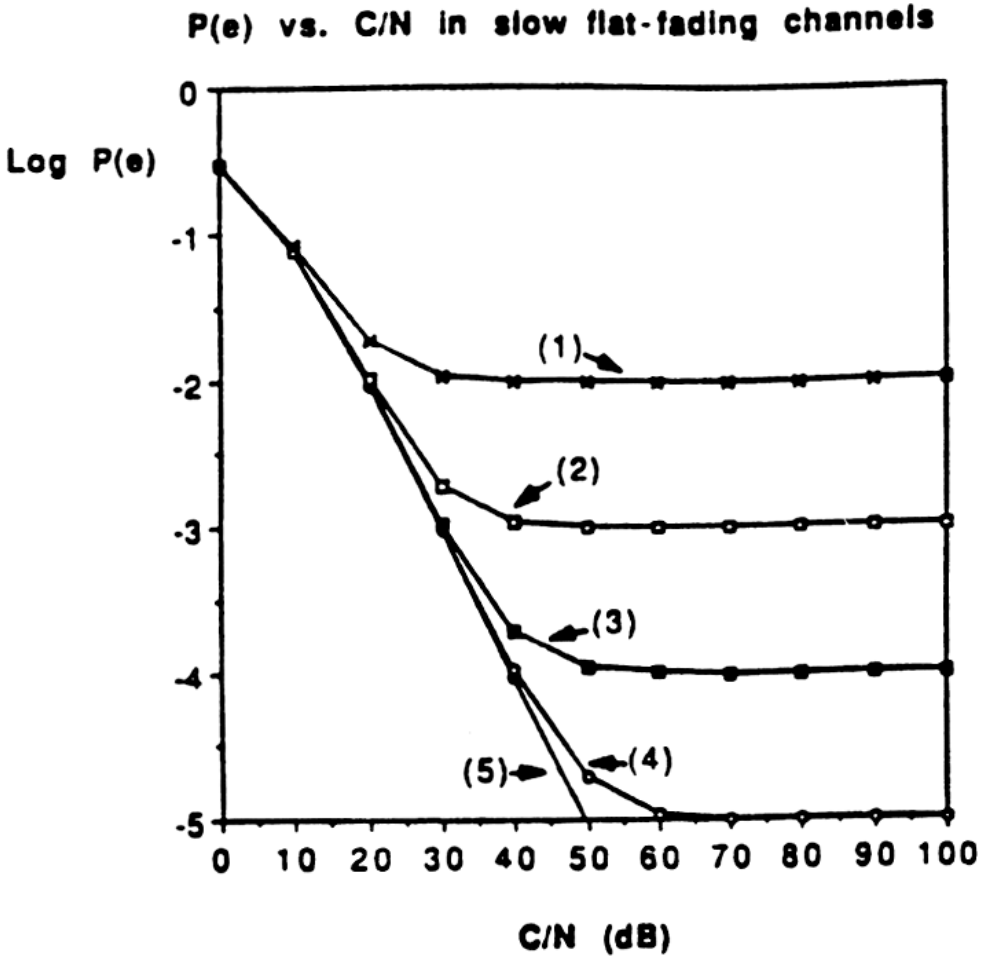

Figure 6.57 BER performance of π/4 DQPSK in a slow flat-fading channel corrupted by CCI and AWGN. f_c = 850 MHz, f_s = 24 ksps raised cosine roll-off factor = 0.2, C/I = (1) 20 dB, (2) 30 dB, (3) 40 dB, (4) 50 dB, (5) infinity [from [Liu91] © IEEE].

Irreducible BER due to fading

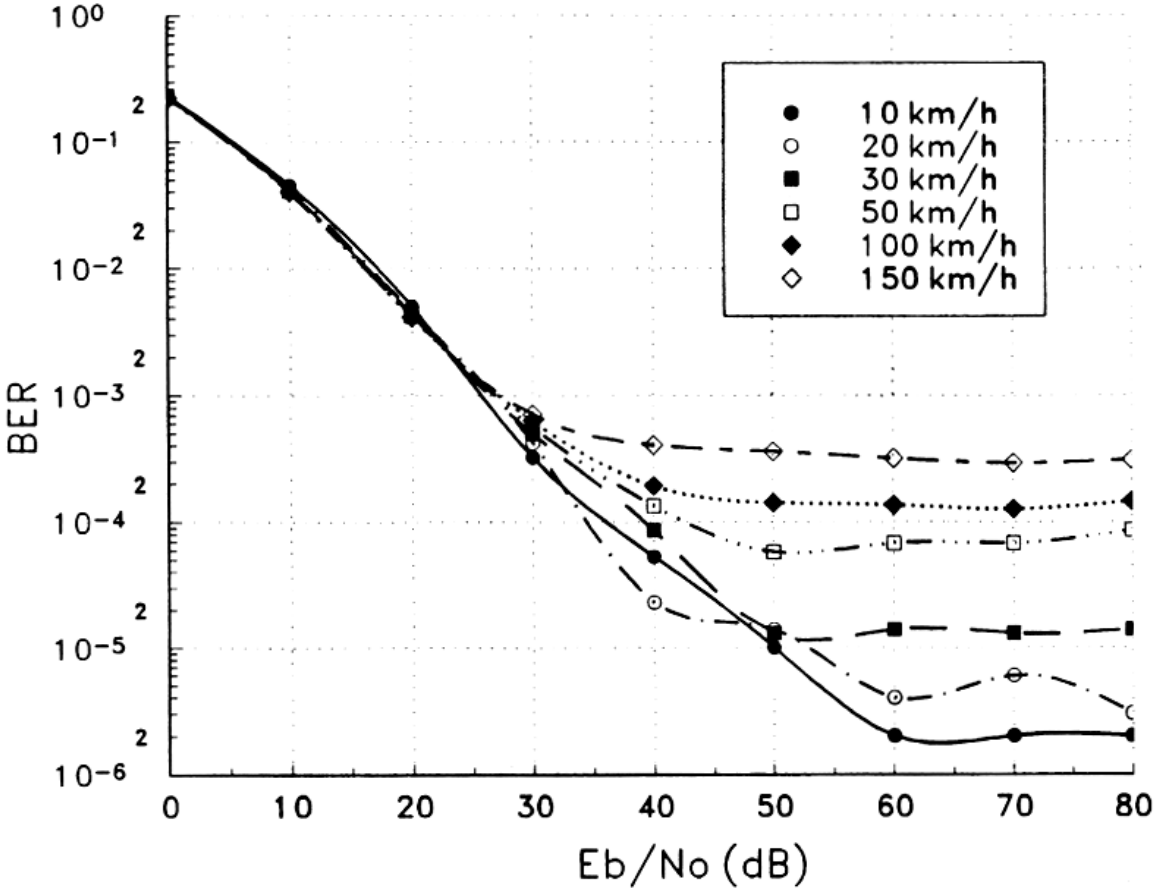

Figure 6.58 BER performance versus E_b / N_0 for $\pi/4$ DQPSK in a Raleigh flat-fading channel for various mobile speeds: $f_c = 850$ MHz, $f_s = 24$ ksps, raised cosine rolloff factor is 0.2, $C/I = 100$ dB. Generated by BERSIM [from [Fun93] © IEEE].

BER due to fading & multipath

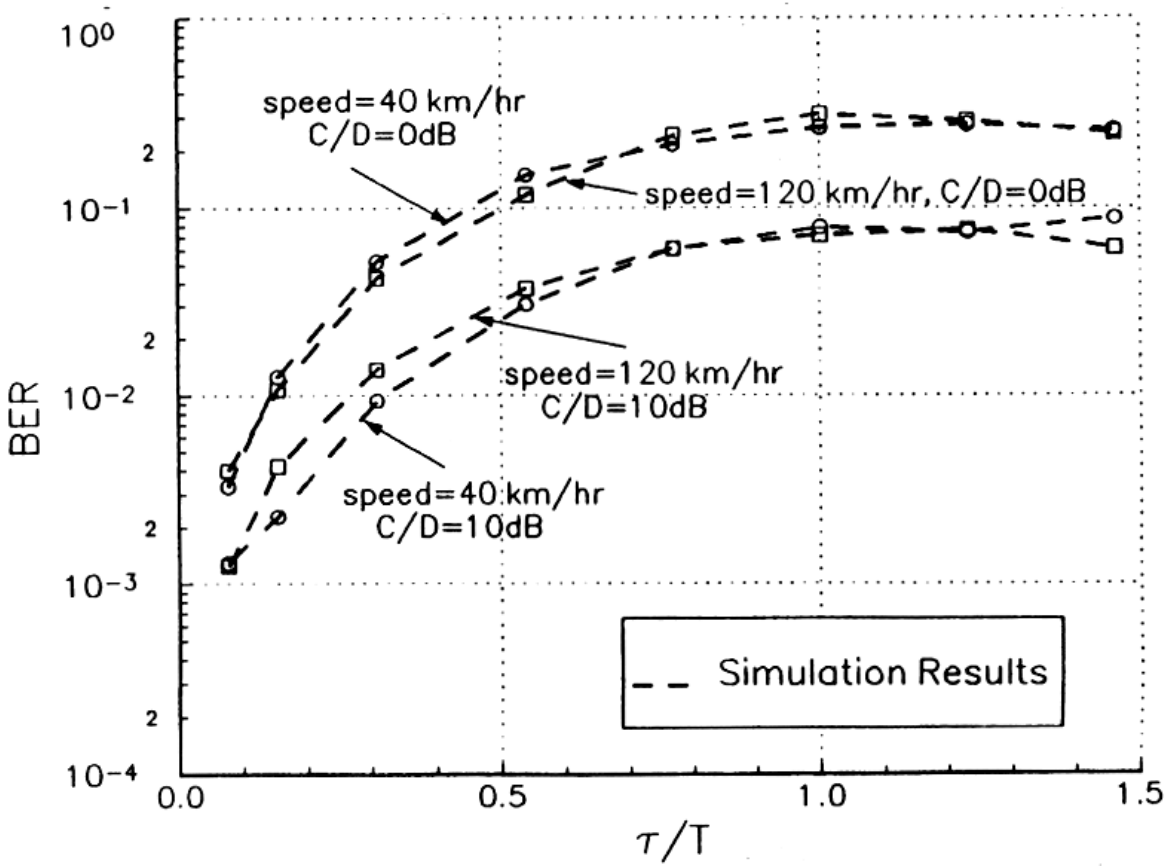

Figure 6.59 BER performance of π/4 DQPSK in a two-ray Rayleigh fading channel, where the time delay τ, and the power ratio *C/D* between the first and second ray are varied. f_c = 850 MHz, f_s = 24 ksps, raised cosine rolloff rate is 0.2, v = 40 km/hr, 120 km/hr E_b/N_0 = 100 dB. Produced by BERSIM [from [Fun93] © IEEE].